

Phenalenyl-Based Highly Conductive Molecular Systems with Hydrogen-Bonded Networks: Synthesis, Physical Properties, and Crystal Structures of 1,3- and 1,6-Diazaphenalenes, and Their Protonated Salts and Charge-Transfer Complexes with TCNQ[1]

Tsuyoshi Murata,[1] Yasushi Morita,*[1,2] Kozo Fukui,[2] Koichi Tamaki,[3] Hideki Yamochi,[4] Gunzi Saito,[5] and Kazuhiro Nakasuji*[1]

[1]Department of Chemistry, Graduate School of Science, Osaka University, 1-1 Machikaneyama, Toyonaka, Osaka 560-0043

[2]PRESTO, Japan Science and Technology Agency (JST), 4-1-8 Honcho, Kawaguchi 332-0012

[3]Department of Functional Molecular Science, Graduate University of Advanced Studies, 38 Nishigounaka, Myodaiji, Okazaki 444-8585

[4]Research Center for Low Temperature and Materials Science, Kyoto University, Oiwake-cho, Kitashirakawa, Sakyo-ku, Kyoto 606-8502

[5]Division of Chemistry, Graduate School of Science, Kyoto University, Oiwake-cho, Kitashirakawa, Sakyo-ku, Kyoto 606-8502

Received November 28, 2005; E-mail: morita@chem.sci.osaka-u.ac.jp

Protonated salts and charge-transfer complexes of the 1,3- and 1,6-diazaphenalene (DAP) systems **5**–**7** have been investigated for new conducting molecule-based materials. Cyclic voltammetry measurements revealed that DAP derivatives are stronger electron donors than hydroquinone, and some of them possess comparable electron-donating abilities to TTF. X-ray crystal structure analyses of HX ($X = Br^-$ and BF_4^-) salts of **5b**, **5c**, and **6e** confirmed their one-dimensional structures by N–H···X···H–N hydrogen bonds and their ability to form hydrogen-bonded networks in charge-transfer complexes. Actually, in the TCNQ salts of protonated **5c**·H^+ and **7b**·H^+, N–H···N≡C hydrogen-bonding interactions between DAP molecules and TCNQ molecules constructed a characteristic hydrogen-bonded cyclic tetramer and linear D–A–D triad, respectively. On the other hand, TCNQ complexes of 1,3- and 1,6-DAP derivatives, prepared by a conventional mixing method of each neutral component, were found to be partial charge-transfer complexes with segregated stacking columns as elucidated from IR and electronic spectra. Their compressed pellets exhibited high electrical conductivity (10^{-2}–10^{-1} S cm^{-1}) at room temperature with semiconducting behavior (activation energy, E_a = 40–80 meV).

The phenalenyl **1a** is a highly-symmetric odd-alternant hydrocarbon π-electronic system with a nonbonding molecular orbital (NBMO), and its three redox species, cation, radical, and anion, possess high thermodynamic stability.[2] In view of the recent growing studies for the construction of molecule-based organic materials such as organic magnets[3] and organic conductors,[4,5] these electronic features of phenalenyl systems have attracted much attention. Haddon and co-workers have demonstrated the phenalenyl-based molecular conductors in the charge-transfer (CT) complexes of 1,9-dithiophenalenyl system **2** with 7,7,8,8-tetracyanoquinodimethane (TCNQ) and its derivative ($\sigma_{rt} = \approx 10^{-2}$ S cm^{-1}),[6] and the spiro-conjugated bisphenalenyl systems **3** ($\sigma_{rt} = 10^{-1}$–10^{-2} S cm^{-1}) as single-component organic conductors.[7]

Our interest in this phenalenyl system was strongly inspired by its highly amphoteric nature related to the NBMO.[2] We designed and synthesized multi-stage amphoteric redox systems with extended conjugated π-electronic networks based on the phenalenyl system.[8] Furthermore, we accomplished the first characterization of the three redox states by introduction of both electron-donating and -withdrawing substituents into the phenalenyl system **4**.[9] These results encouraged us to design and synthesize a variety of phenalenyl-based open-shell molecular systems such as the tri-*t*-butylated phenalenyl **1b**•,[10] oxophenalenoxyl[11] systems, and triangulene[12] (Chart 1).

1,3- and 1,6-Diazaphenalene (DAP) systems are typical examples of heteroatom modifications for the phenalenyl system, in which two nitrogen atoms are incorporated at α positions of the phenalenyl skeleton.[13,14] Their electronic structures are isoelectronic with the phenalenyl anion (**1a**$^-$), indicating that DAP systems are electron-rich systems and can behave as electron-donor molecules in CT complexes. Actually, Pozharskii et al. prepared CT complexes of 1,3-DAP derivatives with electron-acceptors such as 2,3-dichloro-5,6-dicyano-1,4-benzoquinone (DDQ), trinitrobenzene (unknown structure in Ref. 15), *p*-nitrobenzaldehyde, and 1-chloro-2,4-dinitrobenzene, though their solid-state properties such as electrical conductivity were not investigated.[15,16] As for 1,6-DAP, a number of its deriva-

Published on the web June 6, 2006; doi:10.1246/bcsj.79.894

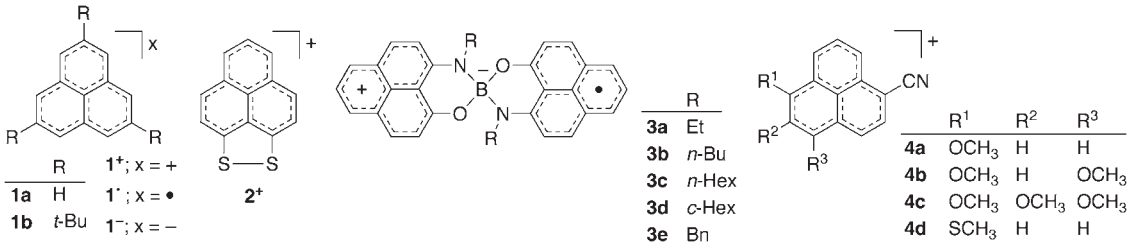

Chart 1. The phenalenyl **1** and phenalenyl-based molecular systems for the molecular conductors **2**–**4**.

tives have been synthesized for medical agents with anti-malaria activities by Cook et al.[17] However, preparation of CT complexes of 1,6-DAP derivatives have not been reported.

In addition to these electronic properties, we have been strongly intrigued by the proton-donor and -acceptor functionalities inherent to DAP systems and their high potentials for forming intermolecular hydrogen bonds (H-bonds) in the solid state.[18,19] These electronic and structural features suggest that DAP systems are good candidates for the electron-donor molecules of H-bonded CT complexes, which have played crucial roles for the studies of cooperative proton–electron transfer systems[20] and for the creation of new organic conductors by structural[21] and electronic[22,23] modulations in CT salts and complexes. With the aim of investigating these roles of the H-bond, we have synthesized H-bonded electron-donor molecules such as tetrathiafulvalene (TTF) derivatives having nucleobases,[24] a hydroxyphenylthio-group,[25] and tris(alkylamino)phenalenylium salt[26] and oligo(imidazole)s.[27]

In this article, we have disclosed new phenalenyl-based organic conductors having H-bonded networks in TCNQ salts and complexes of 1,3- and 1,6-DAP systems as electron-donor molecules, and discussed their electronic and crystal structures on the basis of electron-donating abilities and directionalities of the H-bonds of DAP systems. The relatively high electrical conductivity ($\sigma_{rt} = 10^{-2}$–10^{-1} S cm^{-1}) of TCNQ complexes and robust H-bonding structures have turned out the high potential of 1,3- and 1,6-DAP systems as new molecular systems in molecular-based conductors with a controllable manner of molecular aggregation and electronic structures.

Results

Syntheses of 1,3- and 1,6-DAPs. The 1,3-DAPs **5a**,[14] **5b**,[28] and **5c**[18c] were prepared from 1,8-diaminonaphthalene by condensation with corresponding aldehydes, followed by dehydrogenation using Pd/C catalyst. The 2,5-dichloro-1,6-DAP (**6e**) was synthesized in 5 steps by the reported procedure by Cook et al.[17a–c] The unsubstituted 1,6-DAP (**6a**) was prepared by dechlorination of **6e** with hydrazine monohydrate in the presence of Pd/C catalyst.[17c] A halogenation of **6a** with bromine or *N*-iodosuccinimide (NIS) afforded the 7-bromo and 7-iodo derivatives **6b** or **6c**, respectively.[17d,e] The 7-methoxy derivative **6d** and the new 7,9-dichloro-2-methyl-5-R^2 derivatives **7a**–**7c** (R^2 = methyl, phenyl, and 2-pyridyl) were synthesized by the following methods, including one-carbon elongation and cyclization reactions of the 4-methyl-5-aminoquinoline derivatives **8a**[29] and **8b**[30] as key steps: (1) treatment of **8a** with 2 equivalents of LDA and CO_2 gas followed by a successive treatment with $POCl_3$ and hydrazine monohydrate in the presence of Pd/C catalyst gave **6d**;[17c] (2) treatment of

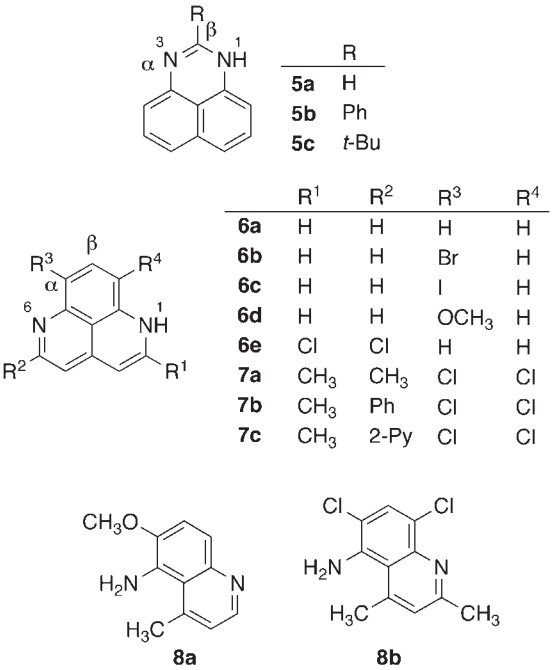

Chart 2. The 1,3- and 1,6-DAP derivatives **5**–**7** described in this article, and synthetic precursors of **6d** and **7**, **8a** and **8b**, respectively.

8b with 2 equivalents of LDA and the corresponding ethyl ester gave **7a**, **7b**, and **7c** in 17, 18, and 41% yields, respectively (Chart 2).

HBr salts of DAPs were prepared by the reaction of DAPs with an excess amount of HBr. The TCNQ$^{\bullet-}$ salts of protonated DAPs were obtained by the metathesis method between the HBr salts of DAPs and Li$^+$TCNQ$^{\bullet-}$ in EtOH. Single crystals of (**5c**$\cdot$H$^+$)(TCNQ$^{\bullet-}$) salt suitable for X-ray structure analysis were obtained by slow concentration of a 150:1 acetone–EtOH solution under continuous Ar-gas flow. Both the aerial evaporation of a MeOH solution of (**7b**$\cdot$H$^+$)(TCNQ$^{\bullet-}$) and the diffusion of a MeOH solution of 1:1 mixture of (**7b**$\cdot$H$^+$)(Br$^-$)–neutral **7b** and Li$^+$TCNQ$^{\bullet-}$ afforded single crystals of a 2:1 salt of (**7b**)(**7b**$\cdot$H$^+$)(TCNQ$^{\bullet-}$)(H$_2$O)$_2$. The TCNQ complexes of DAPs were obtained by the direct method by mixing the solutions of neutral DAPs and TCNQ in THF or $CHCl_3$.

Electrochemical Properties. In order to estimate the electron-donating abilities of 1,3- and 1,6-DAP systems, their electrochemical properties were studied. Figure 1 shows cyclic voltammograms of DAPs (5 or 15 mM solution) in dry DMF containing 0.1 M *n*-Bu$_4$NBF$_4$. Due to the existence of highly acidic N–H moieties, the oxidation processes of all DAP deriv-

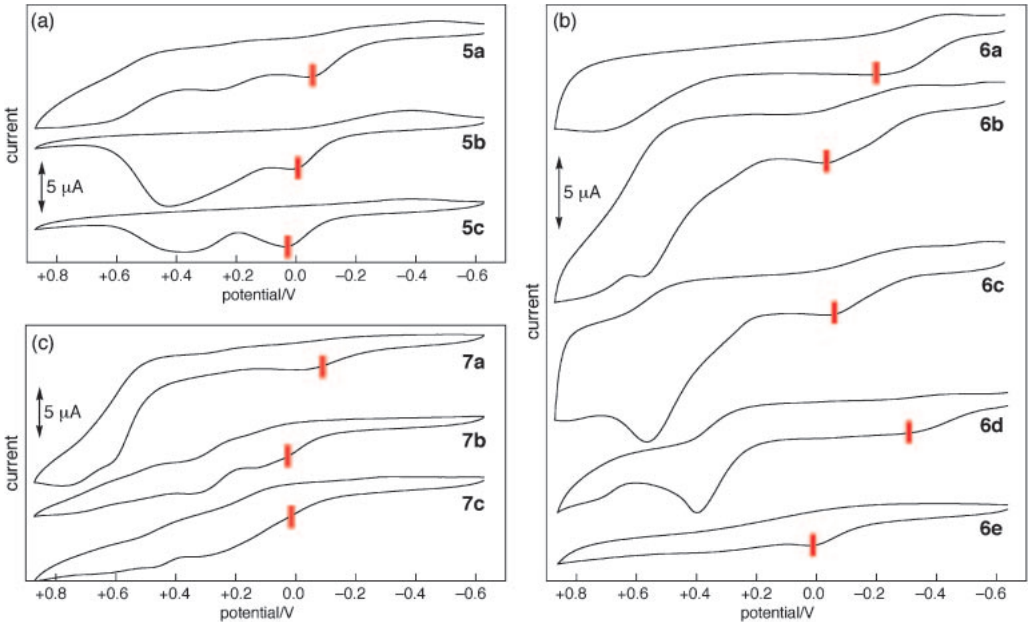

Fig. 1. Cyclic voltammograms (vs Fc/Fc^+) of **5a–5c** (a), **6a–6e** (b), and **7a–7c** (c) in DMF 5 mM for **5a–5c**, **6a–6c**, **7a–7c**, and 15 mM for **6d** and **6e** with 0.1 M $^nBu_4NBF_4$ as the supporting electrolyte at room temperature; sweep rate = 20 mV s^{-1}. The oxidation peaks were pointed by red bars.

Table 1. Oxidation Peak-Potentials of DAPs[a)]

	E_p^{ox}/V		E_p^{ox}/V
5a	−0.04	**6e**	+0.02
5b	+0.02	**7a**	−0.10
5c	+0.04	**7b**	+0.06
6a	−0.20	**7c**	+0.03
6b	−0.02	HQ	+0.26
6c	−0.05	TTF	−0.10
6d	−0.30		

a) Experimental conditions: solvent, DMF; [DAPs] = 5 or 15 mM; [n-Bu_4NBF_4] = 0.1 M; scan rate, 20 mV s^{-1}; reference electrode, $Ag/AgNO_3$ (0.01 M); counter electrode, Pt wire; working electrode, glassy carbon; the results were calibrated with ferrocene/ferrocenium couple.

atives were irreversible, even when the scanning was turned back immediately after the first oxidation potential. Table 1 summarizes their oxidation peak-potentials (E_p^{ox}) calibrated with the ferrocene/ferrocenium couple.

1,3- and 1,6-DAP derivatives were found to be stronger electron-donor molecules than 1,4-hydroquinone (HQ, E_p^{ox} = +0.26 V), and some of the 1,6-DAP derivatives (**6a**, **6d**, and **7a**) exhibited close to or slightly lower oxidation potentials than TTF (E_p^{ox} = −0.10 V). The lower oxidation potential of **6a** than that of **5a** shows that the 1,6-DAP system possesses a stronger electron-donating ability than 1,3-DAP. The phenyl and *t*-butyl substituents at the 2-position in the 1,3-DAP system (**5b** and **5c**) have almost no influence on their oxidation potentials, while methoxy (**6d**) and halogen substituents (**6b**, **6c**, **6e**, and **7a–7c**) in the 1,6-DAP system effectively decreased and increased their oxidation potentials, respectively, due to their electron-donating and -withdrawing effects.

H-Bonding Nature of 1,3- and 1,6-DAP Systems. It is of great importance to elucidate the H-bonding nature of DAPs in the solid state. Figure 2 shows the infrared spectra of 1,3- and 1,6-DAPs measured by KBr pellets and tetrachloroethylene solutions (<1 mM). In Table 2, the N–H stretching frequencies in the solid state (ν_{solid}), those in the solution ($\nu_{solution}$), and the shifted values of ν_{solid} from $\nu_{solution}$ ($\Delta\nu$; $\nu_{solution} - \nu_{solid}$) are summarized. In the case of **5a**, **5b**, and **6a–6e** in the solid states, broad absorption bands were observed at around 2500–3300 cm^{-1}. There are great differences between ν_{solid} and $\nu_{solution}$ in **5a–5c** and **6a–6e**, indicating that they form strong intermolecular H-bonds in the solid state. With the increase of the bulkiness of substituents at the 2-positions in **5a–5c**, the values of ν_{solid} have increased accordingly. These observations can be explained by a steric repulsion of the substituents at the 2-position. Similar to 1,3-DAPs, the 1,6-DAPs **6b–6e** exhibited larger ν_{solid} values (≈200 cm^{-1}) than that of **6a**. The ν_{solid} in **7a–7c** were very close to $\nu_{solution}$, indicating that they possess very weak or almost no intermolecular H-bonding in the solid state. The relatively low $\nu_{solution}$ value of the 2-pyridyl substituted **7c** compared to **7a** and **7b** implies the formation of an intramolecular H-bond between the amino group on the DAP moiety and a nitrogen atom on the pyridine-ring. In the solid-state IR spectra for all HBr salts of 1,3- and 1,6-DAPs, broad N–H stretching absorption bands spread over 2500–3300 cm^{-1}, indicating the formation of N–H···Br H-bondings (Fig. 3).

X-ray Crystal Structure Analysis of Neutral and Protonated Salts of DAPs. In order to investigate the H-bonding natures of 1,3- and 1,6-DAP systems more precisely, we have carried out X-ray crystal structure analyses of neutral **5c** and (**7b**)(CH_3OH), protonated salts (**5b**·H^+)(Br^-), (**5c**·H^+)(Br^-), (**5c**·H^+)(BF_4^-), and (**6e**·H^+)(Br^-). Their crystal data and the experimental details of the structure determination are listed in Table 3. Furthermore, Tables 4 and 5 summarize the

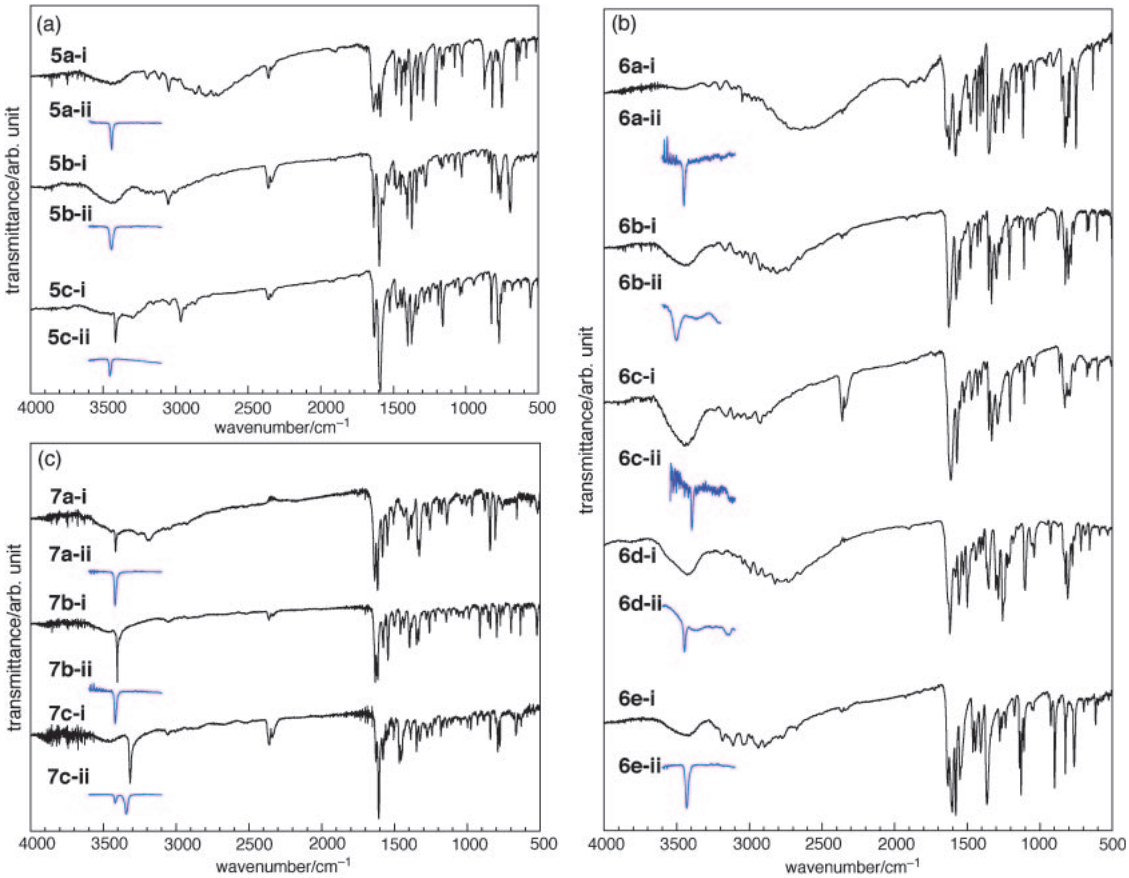

Fig. 2. IR spectra of **5a**–**5c** (a), **6a**–**6e** (b), and **7a**–**7c** (c) in KBr pellets (i, black) and in tetrachloroethylene solutions (ii, blue, <1 mM).

Table 2. The N–H Stretching Frequencies of DAPs

	ν_{solid}[a)]/cm^{-1}	$\nu_{solution}$[b)]/cm^{-1}	$\Delta\nu$/cm^{-1}
5a	2794	3442	648
5b	3150	3443	293
5c	3415, 3300	3452	37, 152
6a	2649	3450	801
6b	2806	3416	610
6c	2926	3397	471
6d	2824	3446	622
6e	2942	3431	489
7a	3415	3419	4
7b	3405	3418	13
7c	3316	3341, 3418	25, 102

a) KBr pellet. b) <1 mM $Cl_2C{=}CCl_2$ solution.

selected intramolecular bond lengths of 1,3-DAP and 1,6-DAP systems, respectively.

2-*t*-Butyl-1,3-DAP (5c): Within a unit cell, there were two crystallographically independent molecules (**5c**-A and **5c**-B) (Fig. 4a). The C–C bond lengths in the naphthalene skeletons of **5c**-A and **5c**-B molecules were similar to those of naphthalene (e, f, n, m = 1.426 Å, h, g, l, k = 1.378 Å, j, i = 1.415 Å, and o = 1.426 Å in Table 4),[31] and showed no remarkable bond alternation. While, the C1–N1 and C1–N2 bond lengths in the pyrimidine skeleton in both **5c**-A and **5c**-B molecules exhibited bond alternation (Table 4). This clearly shows that double-bonds in the pyrimidine skeleton localize at the C1A–N2A bond in **5c**-A and C1B–N2B bond in **5c**-B, and that **5c** forms very weak or no intermolecular H-bond in the solid state. Actually, the closest intermolecular N1A···N2B distance (3.33 Å) was longer than the sum of the van der Waals radius of two nitrogen atoms (3.10 Å).[32] Thus, the N–H···N H-bond in **5c** in the solid state is very weak, and this result is in agreement with the IR study. The **5c**-A molecules formed a dimeric structure with a long face-to-face distance of 4.67 Å (Fig. 4b). These weak dimerization and weak H-bonds formed a tetramer unit (Fig. 4c) in which the angle between the neighboring **5c**-A and **5c**-B was 89.2°. Noticeable intermolecular interactions were not found between the tetramer units (Fig. 4d).

7,9-Dichloro-2-methyl-5-phenyl-1,6-DAP [(7b)(CH_3OH)]: This crystal consisted of neutral **7b** and MeOH molecules. The phenyl group was twisted from the nearly planar DAP skeleton by 37° (Fig. 5a). In the intramolecular C–C and C–N bond lengths, the DAP skeleton showed no noticeable bond alternation and possessed nearly C_2 symmetry (Table 5). The **7b** molecule stacked with inverted arrangements, resulting in the formation of a one-dimensional column (Figs. 5b–5d). Within this column, neighboring **7b** molecules were connected by two sets of H-bonds via MeOH molecules to form face-to-face dimers (Figs. 5b and 5c). The H-bonding lengths were 2.89 Å (N1···O1) and 2.98 Å (N2···O1). The interplanar distance of the H-bonded face-to-face dimer (3.49 Å) was slightly longer than that between dimers (3.37 Å). There were no noticeable intermolecular interactions between one-dimensional columns.

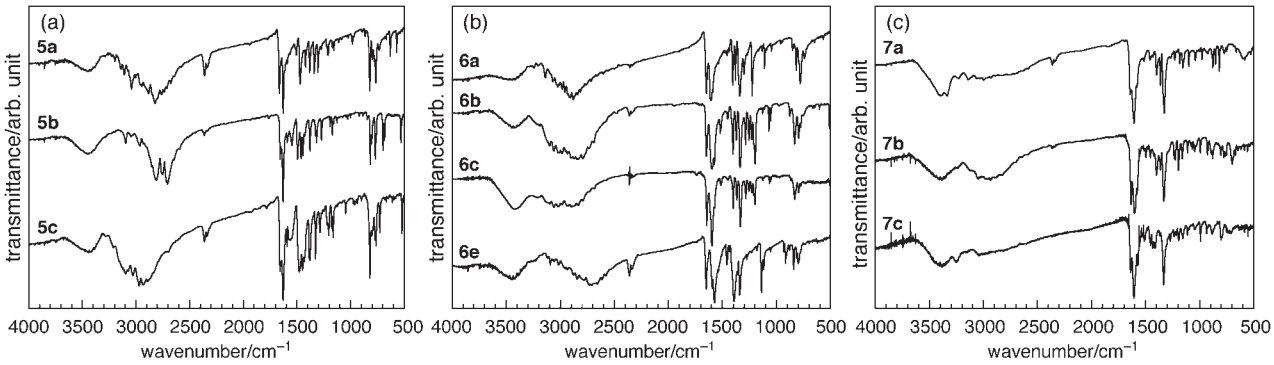

Fig. 3. IR spectra of HBr salts of **5a**–**5c** (a), **6a**–**6c** and **6e** (b), and **7a**–**7c** (c) in KBr pellets.

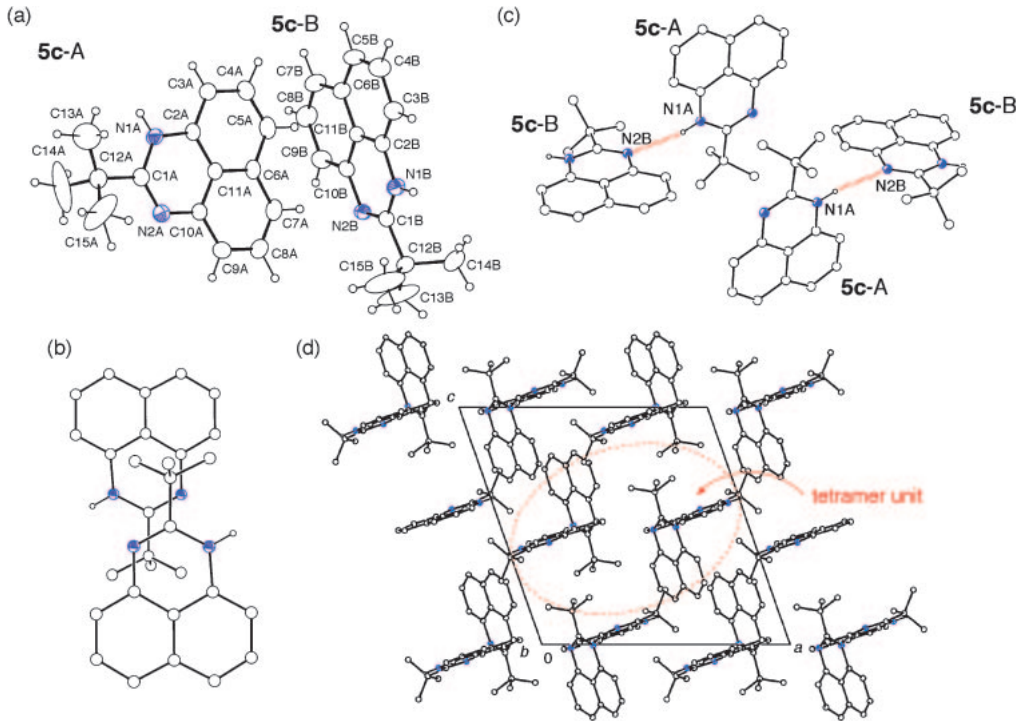

Fig. 4. Crystal structure of **5c**. Molecular structure and atomic numbering scheme (a). Overlap mode of the dimer of **5c**-A with a face-to-face distance of 4.67 Å (b). Tetramer unit formed by weak H-bonding and weak dimerization (c). Perspective view of the crystal packing along the *b*-axis. The dashed ellipse illustrates the tetramer unit (d).

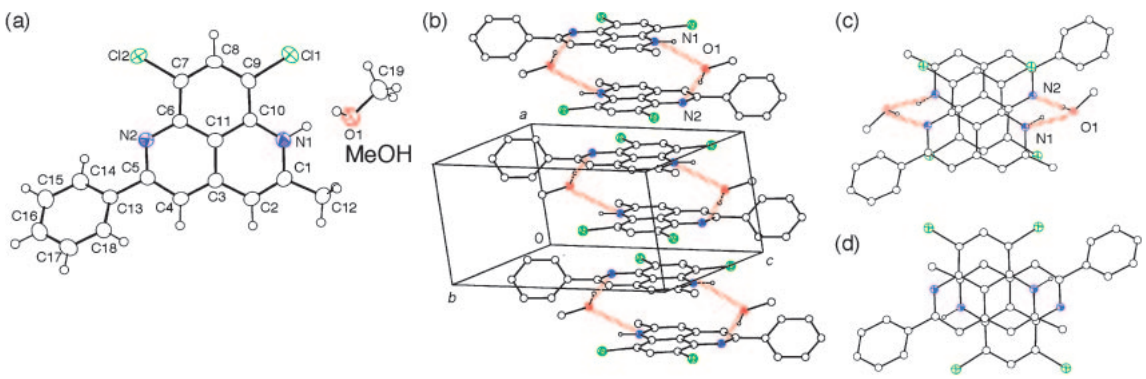

Fig. 5. Crystal structure of (**7b**)(MeOH). Molecular structure and atomic numbering scheme (a). One-dimensional columnar structure along the *a*-axis by π-stacking and double H-bonding interaction across MeOH (b). Overlap mode of the π-stacking column within and between the H-bonded dimer (c) and (d), respectively.

Table 3. Crystal Data for Neutral DAP, Protonated DAP, and TCNQ Salts of Protonated DAPs

	5c	(**7b**)(CH_3OH)	(**5b**·H^+)(Br^-)	(**5c**·H^+)(Br^-)	(**5c**·H^+)(BF_4^-)	(**6e**·H^+)(Br^-)	(**5c**·H^+)($TCNQ^{\bullet -}$)$(H_2O)_{0.5}$	(**7b**)(**7b**·H^+)$(TCNQ^{\bullet -})(H_2O)_2$
Crystal formula	$C_{15}H_{16}N_2$	$C_{19}H_{16}Cl_2N_2O$	$C_{17}H_{13}BrN_2$	$C_{15}H_{17}BrN_2$	$C_{15}H_{17}BF_4N_2$	$C_{11}H_7BrCl_2N_2$	$C_{26}H_{22}N_6O_{0.5}$	$C_{48}H_{33}Cl_4N_8O_2$
Formula weight	224.30	343.25	325.21	305.22	312.12	318.00	438.51	895.65
Crystal habit	yellow, columnar	yellow, columnar	orange, platelet	yellow, block	yellow, columnar	orange, columnar	black, block	black, needle
Crystal system	monoclinic	triclinic	orthorhombic	triclinic	monoclinic	monoclinic	triclinic	monoclinic
Space group	$P2_1/n$ (#14)	$P\bar{1}$ (#2)	$Pbcn$ (#60)	$P\bar{1}$ (#2)	$P2_1/n$ (#14)	$C2/c$ (#15)	$P\bar{1}$ (#2)	$C2/c$ (#15)
a/Å	14.302(2)	7.342(10)	8.102(3)	11.671(3)	20.85(3)	10.338(4)	8.959(5)	41.53(2)
b/Å	12.952(2)	9.24(1)	24.314(3)	14.457(4)	6.676(8)	14.469(2)	9.847(6)	3.799(1)
c/Å	14.464(1)	13.40(2)	7.169(2)	8.733(2)	20.78(2)	15.665(2)	14.660(9)	26.54(1)
α/deg		84.39(4)		99.28(2)			104.71(3)	
β/deg	109.274(6)	77.00(4)		106.99(2)	92.35(4)	97.85(2)	98.91(3)	99.95(2)
γ/deg		68.79(4)		80.40(2)			101.87(3)	
V/Å^3	2529.0(4)	825(7)	1412.4(6)	1379.5(6)	2889(21)	2321.2(7)	1194(4)	4124(2)
Z	8	2	4	4	8	8	2	4
D_{calcd}[a)]/g cm^{-3}	1.178	1.381	1.529	1.469	1.435	1.820	1.219	1.442
Temperature/K	296	200	296	296	200	296	296	150
μ(Mo Kα)/cm^{-1}	0.70	3.93	29.09	29.73	1.20	39.82	0.77	3.40
Unique reflections	6068	3690	1628	6338	6602	3524	5131	4280
Reflections used	2941[b)]	2652[c)]	878[b)]	4255[b)]	3170[d)]	1789[c)]	3482[b)]	2481[b)]
Refined parameters	363	217	98	461	397	146	318	275
R, Rw	0.066, 0.077	0.042, 0.111	0.031, 0.032	0.033, 0.034	0.069, 0.151	0.046, 0.048		
$R1$, $wR2$							0.092, 0.333	0.073, 0.240
GOF	2.99	1.75	1.51	1.81	1.00	1.91	1.28	0.96

a) D_{calcd} is calculated density. b) $I > 2.00\sigma(I)$. c) $I > 3.00\sigma(I)$. d) $I > 0.50\sigma(I)$.

Table 4. C–C and C–N Bond Lengths of DAP Skeletons in the Crystal Structures of **5c**, (**5b**·H$^+$)(Br$^-$), (**5c**·H$^+$)(Br$^-$), (**5c**·H$^+$)(BF$_4^-$), and (**5c**·H$^+$)(TCNQ$^{\bullet-}$)(H$_2$O)$_{0.5}$

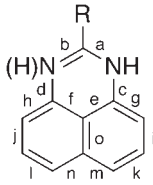

	R
5b	Ph
5c	*t*-Bu

	5c		(**5b**·H$^+$)(Br$^-$)	(**5c**·H$^+$)(Br$^-$)		(**5c**·H$^+$)(BF$_4^-$)		(**5c**·H$^+$)(TCNQ$^{\bullet-}$)
	5c-A	**5c**-B		**5c**·H$^+$-A	**5c**·H$^+$-B	**5c**·H$^+$-A	**5c**·H$^+$-B	(H$_2$O)$_{0.5}$
a	1.369(4)	1.365(4)	1.331(4)	1.323(3)	1.329(3)	1.332(8)	1.318(8)	1.320(3)
b	1.291(4)	1.296(4)	—	1.325(3)	1.319(3)	1.335(9)	1.310(8)	1.311(3)
c	1.402(4)	1.396(4)	1.411(4)	1.412(4)	1.417(4)	1.430(8)	1.428(8)	1.419(3)
d	1.403(4)	1.415(4)	—	1.411(4)	1.421(4)	1.409(8)	1.430(7)	1.403(3)
e	1.408(4)	1.403(4)	1.406(4)	1.408(4)	1.405(4)	1.382(9)	1.395(9)	1.404(5)
f	1.418(4)	1.426(4)	—	1.410(4)	1.410(4)	1.415(8)	1.415(9)	1.402(3)
g	1.368(4)	1.365(5)	1.365(4)	1.368(4)	1.366(4)	1.367(9)	1.390(9)	1.354(3)
h	1.373(5)	1.376(5)	—	1.365(4)	1.366(4)	1.342(9)	1.348(9)	1.374(3)
i	1.406(5)	1.396(6)	1.408(6)	1.400(4)	1.402(4)	1.405(9)	1.410(9)	1.407(4)
j	1.411(6)	1.398(5)	—	1.404(4)	1.405(5)	1.421(9)	1.414(9)	1.409(4)
k	1.357(5)	1.368(6)	1.352(5)	1.362(4)	1.357(4)	1.370(10)	1.363(10)	1.353(4)
l	1.352(6)	1.352(6)	—	1.352(5)	1.356(5)	1.363(10)	1.352(10)	1.333(4)
m	1.410(5)	1.418(5)	1.410(5)	1.410(4)	1.416(4)	1.421(9)	1.432(10)	1.407(4)
n	1.417(5)	1.411(5)	—	1.420(4)	1.424(4)	1.414(10)	1.422(10)	1.417(4)
o	1.423(4)	1.418(4)	1.421(6)	1.411(4)	1.408(4)	1.421(8)	1.397(8)	1.425(3)

Table 5. C–C and C–N Bond Lengths of DAP Skeletons in the Crystal Structures of (**7b**)(MeOH), (**6e**·H$^+$)(Br$^-$), and (**7b**)(**7b**·H$^+$)(TCNQ$^{\bullet-}$)(H$_2$O)$_2$

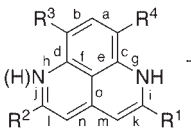

	R^1	R^2	R^3	R^4
6e	Cl	Cl	H	H
7b	CH_3	Ph	Cl	Cl

	(**7b**)(MeOH)	(**6e**·H$^+$)(Br$^-$)	(**7b**)(**7b**·H$^+$)(TCNQ$^{\bullet-}$)(H$_2$O)$_2$
a	1.389(3)	1.376(7)	1.390(5)
b	1.370(3)	1.388(8)	1.376(5)
c	1.383(3)	1.400(7)	1.389(6)
d	1.412(3)	1.383(7)	1.400(6)
e	1.426(3)	1.408(7)	1.424(5)
f	1.425(3)	1.421(6)	1.416(5)
g	1.380(3)	1.386(6)	1.385(5)
h	1.375(3)	1.370(6)	1.374(5)
i	1.373(3)	1.345(6)	1.351(5)
j	1.337(3)	1.357(6)	1.354(5)
k	1.357(3)	1.350(7)	1.379(6)
l	1.395(3)	1.362(7)	1.385(5)
m	1.436(3)	1.408(7)	1.419(5)
n	1.396(3)	1.404(7)	1.402(6)
o	1.426(3)	1.420(6)	1.428(6)

2-Phenyl-1,3-DAP·H$^+$ Bromide [(5b·H$^+$)(Br$^-$)]: In this crystal, the DAP skeleton of the **5b**·H$^+$ molecule possessed a planar structure with C_{2v} symmetry (Fig. 6a). The phenyl group was twisted by 33.9° from the DAP skeleton at the C1–C8 bond. The neighboring **5b**·H$^+$ molecules were connected by the three-centered H-bonds of N1–H···Br1···H–N1, resulting in the formation of a one-dimensional chain along the *a*-axis (Fig. 6b). The N1···Br1 distance was 3.23 Å. The neighboring **5b**·H$^+$ planes in a H-bonded chain were parallel. The **5b**·H$^+$ molecule stacked with a face-to-face distance of 3.44 Å to form a uniform π-stacking column along the *b*-axis (Fig. 6c). The phenyl groups were alternately arranged in opposite directions in order to reduce their intermolecular steric repulsion (Fig. 6c).

2-*t*-Butyl-1,3-DAP·H$^+$ Bromide [(5c·H$^+$)(Br$^-$)]: Two crystallographically independent **5c**·H$^+$ (**5c**·H$^+$-A and **5c**·H$^+$-B) and bromide ions (Br1A and Br1B) existed in a unit cell (Fig. 7a). Contrary to the molecular structure of neutral **5c**, the intramolecular C1–N1 and C1–N2 bond lengths in both **5c**·H$^+$-A and **5c**·H$^+$-B molecules were close to each other, which was caused by the charge delocalization on the C–N bonds by the formation of intermolecular H-bonds (Table 4). The **5c**·H$^+$-A and **5c**·H$^+$-B molecules were each linked by independent H-bonding interactions via bromide ions and formed one-dimensional H-bonded chain structures through N–H···Br···H–N H-bonding in a tape-like fashion parallel to the *c*-axis (Figs. 7b and 7c). The N···Br distances in the H-bonded chains were 3.40 (N1A···Br1A), 3.47 (N2A···Br1A), 3.38 (N1B···Br1B), and 3.47 Å (N2B···Br1B). This H-bonding feature was almost identical with that seen in (**5b**·H$^+$)(Br$^-$). The **5c**·H$^+$-A molecule formed a π-stacking dimer to form a pair of H-bonded chains (Fig. 7e). The stacking pattern in the π-stacking dimer was of slipped head-to-tail fashion, and the face-to-face distance was 3.50 Å (Fig. 7d).

2-*t*-Butyl-1,3-DAP·H$^+$ Tetrafluoroborate [(5c·H$^+$)(BF$_4^-$)]: Figure 8a shows the molecular structures of crystallographically independent **5c**·H$^+$ molecules (**5c**·H$^+$-A and **5c**·H$^+$-B) and tetrafluoroborate ions (BF$_4$-A and -B). Similar to those in (**5c**·H$^+$)(Br$^-$), the C–N bond length in **5c**·H$^+$-A and **5c**·H$^+$-B in this salt exhibited no pronounced bond alternation (Table 4).

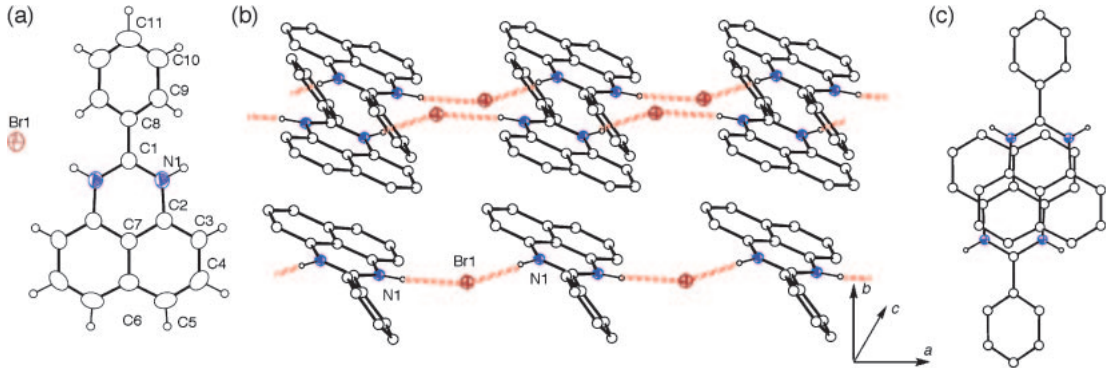

Fig. 6. Crystal structure of (**5b**•H$^+$)(Br$^-$). Molecular structure and atomic numbering scheme (a). One-dimensional chain structure along the *a*-axis N1–H···Br1···H–N1 H-bonds and uniform π-stacking structures along the *b*-axis (b). Overlap mode in the uniform π-stacking column (c).

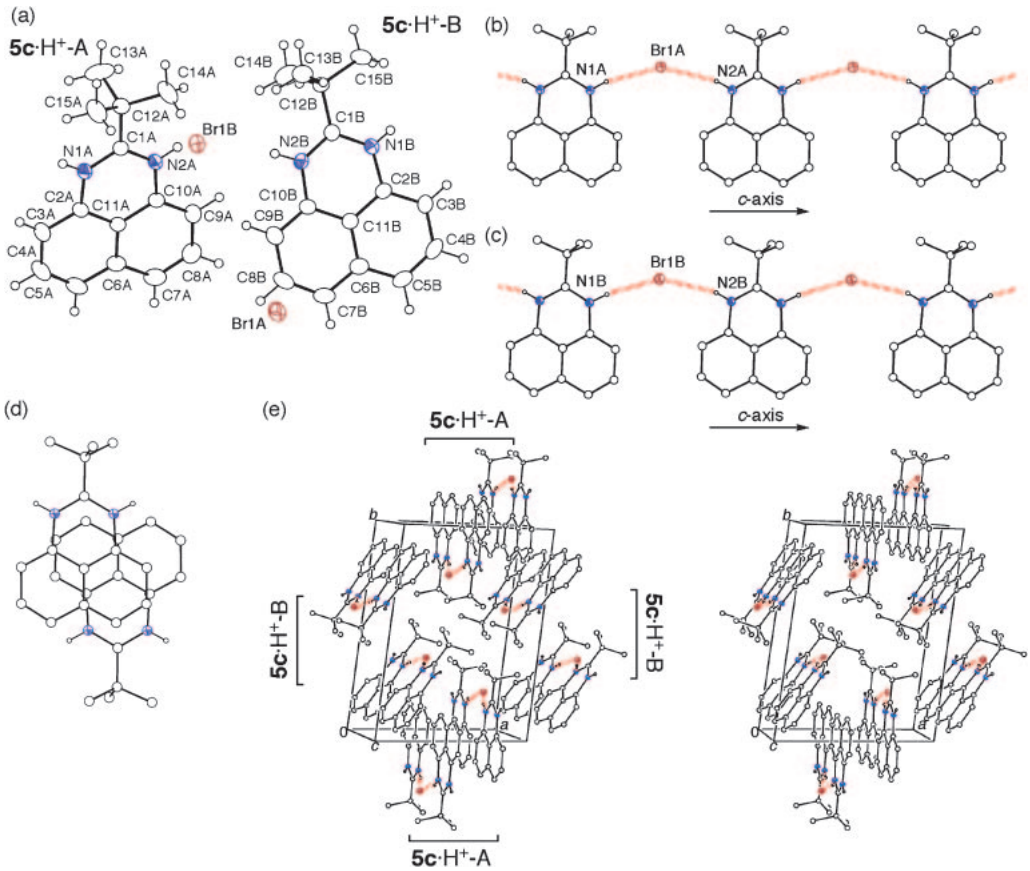

Fig. 7. Crystal structure of (**5c**•H$^+$)(Br$^-$). Molecular structure and atomic numbering scheme (a). One-dimensional chain structure of **5c**•H$^+$-A and -B by N–H···Br···H–N H-bonds along the *c*-axis (b and c, respectively). Overlap mode in a π-stacking dimer of **5c**•H$^+$-A (d). Stereoview of the crystal packing showing the H-bonding and π-stacking interactions (e).

Both **5c**•H$^+$-A and **5c**•H$^+$-B molecules independently stacked in a head-to-tail fashion to form π-stacking columns along the *b*-axis (Figs. 8b–8e). The face-to-face distances in π-stacking columns were 3.3–3.4 Å. Two nitrogen atoms in each molecule formed intermolecular H-bonds with the fluorine atoms of tetrafluoroborate ions in **5c**•H$^+$-A–BF_4-A–**5c**•H$^+$-B–BF_4-B fashion, resulting in the formation of a zigzag H-bonded chain elongated in the [−101] direction (Fig. 8f). The H-bonding lengths were 2.88 (N1A···F1A), 2.89 (N2A···F4B), 2.86 (N1B···F1B), and 2.89 Å (N2B···F4A). These H-bonds connected the neighboring stacking columns to form the three-dimensional network of this crystal.

2,5-Dichloro-1,6-DAP•H$^+$ Bromide [(6e•H$^+$)(Br$^-$)]: This protonated salt consisted of a crystallographycally independent one **6e**•H$^+$ molecule and two bromide ions (Br1A and Br1B on the special positions) (Fig. 9a). The DAP skeleton showed no marked bond-alternation, and the molecular structure possesses nearly C_{2v} symmetry (Table 5). The **6e**•H$^+$ molecules were connected by N1–H···Br1A···H–N1 and N2–H···Br1B···H–N2 H-bonds, resulting in the formation of a one-dimension-

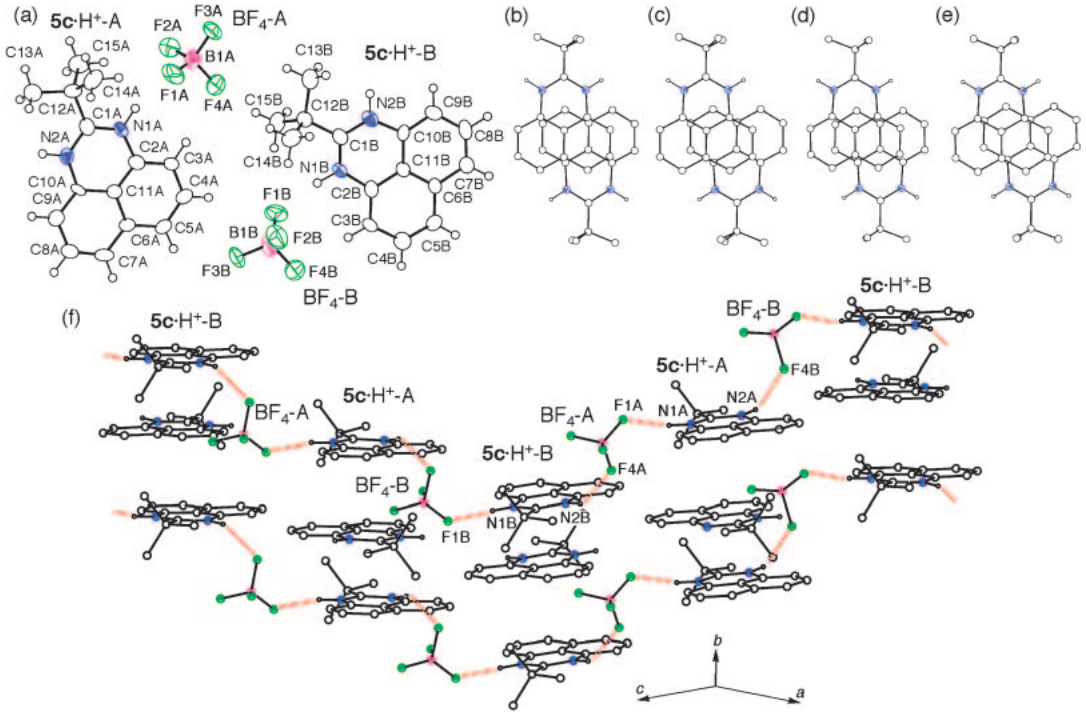

Fig. 8. Crystal structure of (**5c**·H^+)(BF_4^-). Molecular structure and atomic numbering scheme (a). Overlap mode in π-stacking columns of **5c**·H^+-A (b and c) and **5c**·H^+-B (d and e). Molecular packing showing the zigzag-H-bonded chain along the [−101] direction and π-stacking column along the *b*-axis (f).

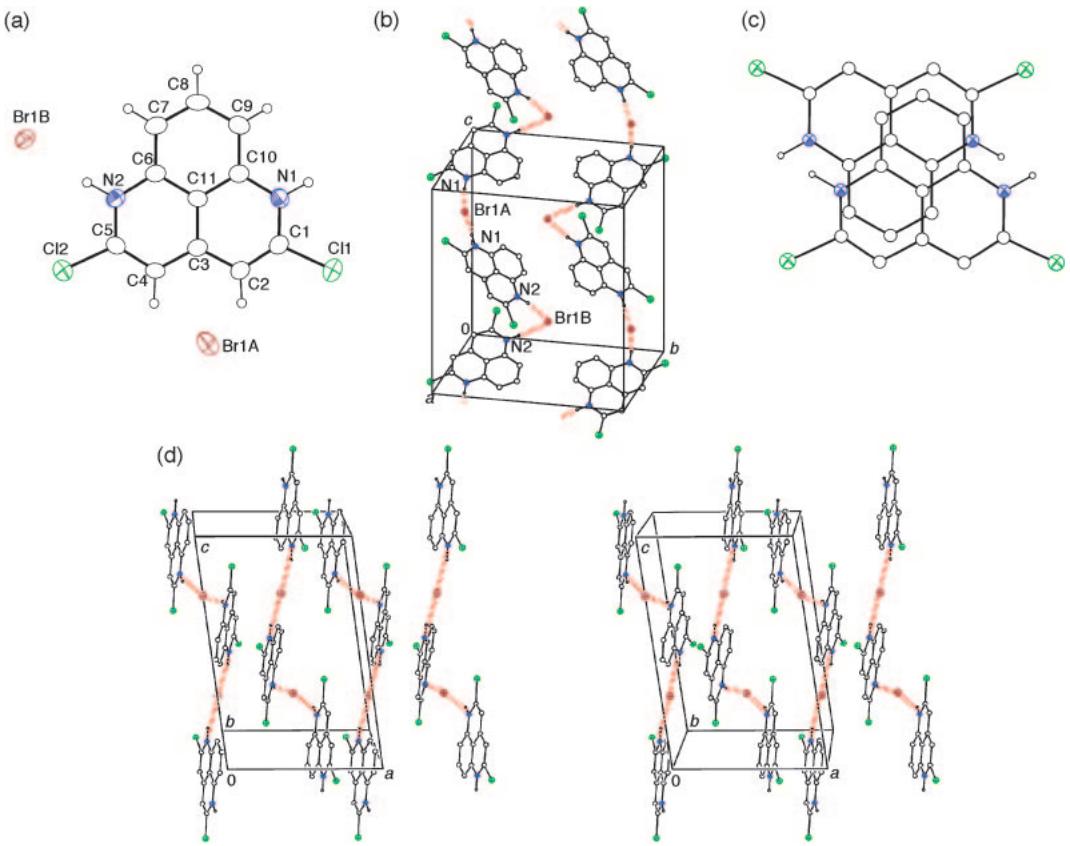

Fig. 9. Crystal structure of (**6e**·H^+)(Br^-). Molecular structure and atomic numbering scheme (a). One-dimensional chain by N–H···Br···H–N H-bond along the *c*-axis (b). Overlap mode of π-stacking dimer (c). Stereoview of the crystal packing showing the H-bonding and π-stacking interactions (d).

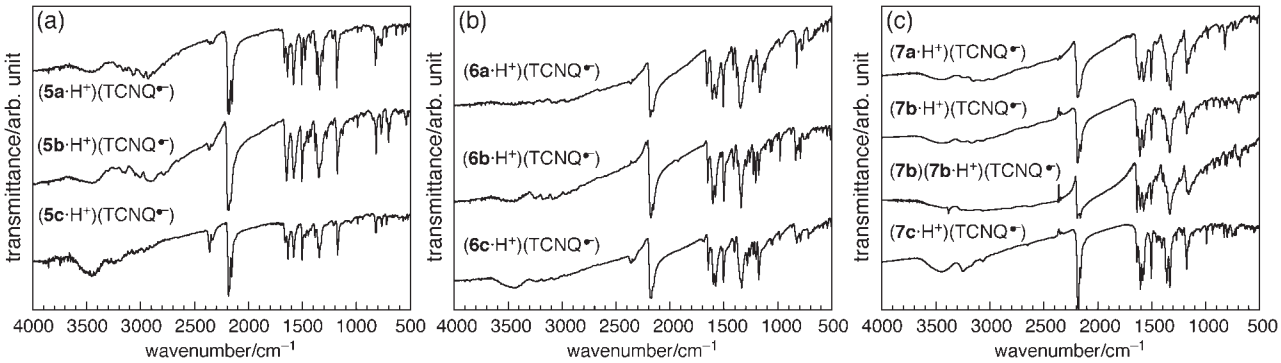

Fig. 10. IR spectra in KBr pellets of (DAP·H$^+$)(TCNQ$^{\bullet-}$) salts: **5a–5c** (a), **6a–6c** (b), and **7a–7c** (c).

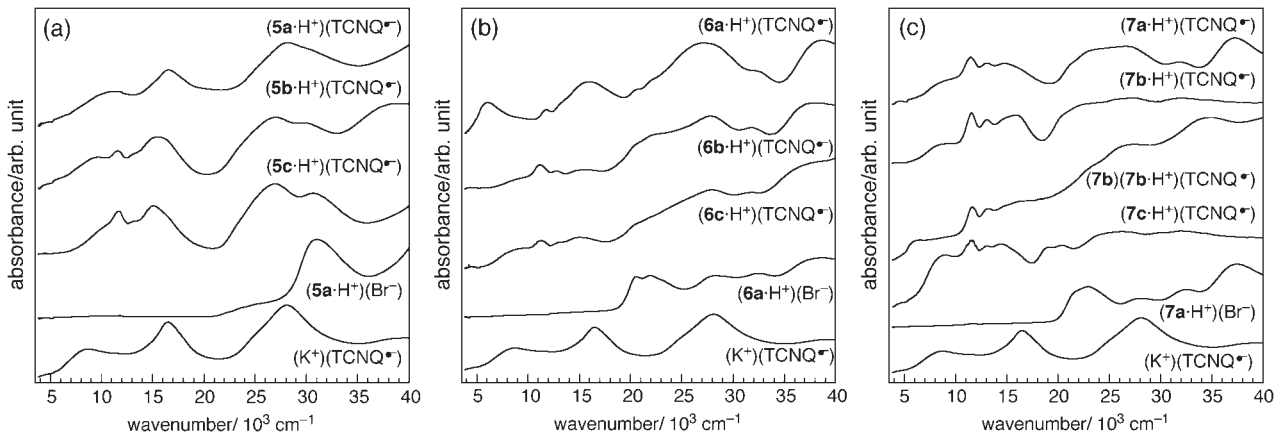

Fig. 11. Electronic spectra in KBr pellets of (DAP·H$^+$)(TCNQ$^{\bullet-}$): **5a–5c** (a), **6a–6c** (b), and **7a–7c** (c).

Table 6. Physical Properties of CT Salts of DAP·H$^+$ with TCNQ$^{\bullet-}$ Prepared by the Metathesis Method

Composition[a]	ν_{CN}[b]/cm^{-1}	N–H stretching frequency/cm^{-1}	B-band[b] /10^3 cm^{-1}	C-band[b] /10^3 cm^{-1}	D-band[b] /10^3 cm^{-1}	F-band[b] /10^3 cm^{-1}
(**5a**·H$^+$)(TCNQ$^{\bullet-}$)(H$_2$O)$_{0.4}$	2191	2927	—[c]	11.4	16.6	28.2
(**5b**·H$^+$)(TCNQ$^{\bullet-}$)(H$_2$O)$_{0.25}$	2196	2905	9.7	11.6	15.5	27.0
(**5c**·H$^+$)(TCNQ$^{\bullet-}$)(H$_2$O)$_{0.5}$	2183	3183, 3244, 3296	9.7sh	11.7	15.1	26.9
(**6a**·H$^+$)(TCNQ$^{\bullet-}$)(H$_2$O)$_{0.25}$	2184	2950	6.1	11.8	16.0	27.2
(**6b**·H$^+$)(TCNQ$^{\bullet-}$)	2178	3180	9.3sh	11.1	15.5	27.8
(**6c**·H$^+$)(TCNQ$^{\bullet-}$)(H$_2$O)$_{0.25}$	2182	3239	8.9sh	11.3	15.0	27.9
(**7a**·H$^+$)(TCNQ$^{\bullet-}$)	2188	3147	8.3sh	11.5	14.7	26.6
(**7b**·H$^+$)(TCNQ$^{\bullet-}$)(C$_2$H$_6$O)$_{0.75}$	2186	3174	9.1	11.5	14.3	27.0
(**7b**)(**7b**·H$^+$)(TCNQ$^{\bullet-}$)(H$_2$O)$_2$	2189	3384, 3066	5.8	11.6	16.2	27.0
(**7c**·H$^+$)(TCNQ$^{\bullet-}$)(H$_2$O)$_{0.25}$	2177	3252	9.1	11.4	14.3	25.9

a) Molar ratio was estimated by the elemental analysis. b) IR and electronic spectra were measured in KBr pellets. c) The peak was not observed.

al chain along the *c*-axis (Fig. 9b). The strongly twisted shape of the H-bonded chain like a two-fold screw structure, which was derived from the small N2···Br1B···N2 angle of 67.19°, was a salient feature of this system. This H-bonded structure was quite different from those of the HBr salts of **5b** and **5c**, which formed planar H-bonded networks. The N1···Br1A and N2···Br1B distances were 3.23 and 3.29 Å, respectively. Two **6e**·H$^+$ molecules stacked in a slipped head-to-tail fashion to form a π-stacking dimer with a stacking distance of 3.40 Å (Fig. 9c). This π-stacking interaction connected the H-bonded chain to form a two-dimensional network parallel to the *ac* plane (Fig. 9d).

Electronic Properties and Crystal Structures of CT Salts of Protonated DAP Cation with TCNQ$^{\bullet-}$. Spectral Features of TCNQ$^{\bullet-}$ Salt: In order to investigate the electronic properties and crystal structures of CT salts of DAPs, we first focus on the TCNQ$^{\bullet-}$ salts of protonated DAPs obtained by the metathesis method. Figures 10 and 11 display IR and electronic spectra of TCNQ$^{\bullet-}$ salts of **5a–5c**, **6a–6c**, and **7a–7c**. Table 6 summarizes their compositions, nitrile stretching frequency, and frequency of CT bands.[33] The molecular ratios of these TCNQ$^{\bullet-}$ salts were estimated to be 1:1 by elemental analysis for all CT salts, except for (**7b**)(**7b**·H$^+$)(TCNQ$^{\bullet-}$)-(H$_2$O)$_2$ salt. All the CT salts showed the nitrile stretching fre-

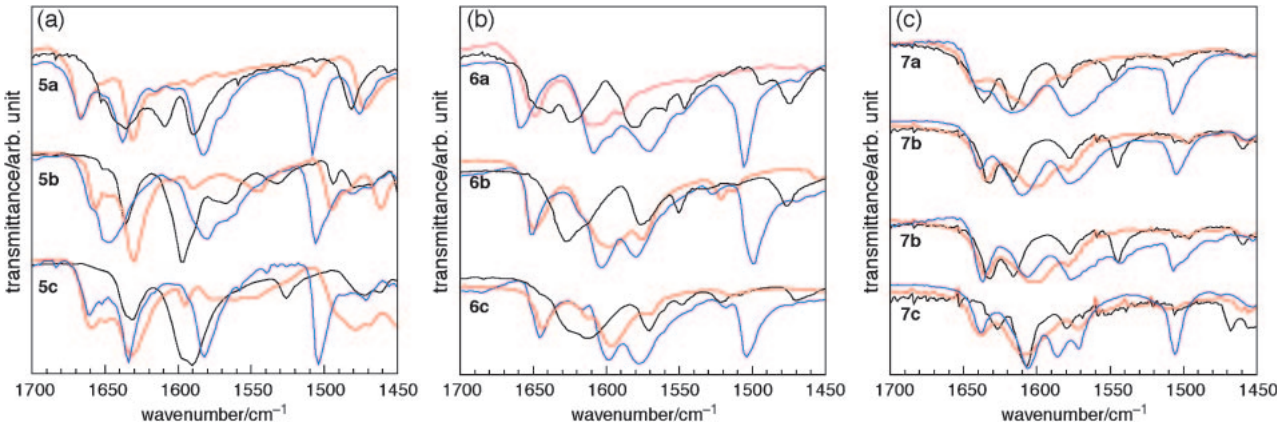

Fig. 12. IR spectra of neutral species (black line), HBr salts (red line), and $TCNQ^{\bullet-}$ salts (blue line) of DAPs **5a**–**5c** (a), **6a**–**6c** (b), and **7a**–**7c** (c) in the frequency range 1450–1700 cm^{-1} measured by KBr pellets.

quency of TCNQ moieties at 2177–2196 cm^{-1}, which indicates the ionic form of the TCNQ moiety in these CT salts (Fig. 10).[34] In the electronic spectra (Fig. 11), these $TCNQ^{\bullet-}$ salts showed a general resemblance to $TCNQ^{\bullet-}$ and 1,3- and 1,6-DAP·H^+ species; the completely ionic salt $K^+TCNQ^{\bullet-}$ exhibits the B- and C-bands (intermolecular transition of $TCNQ^{\bullet-}$) at 8200 and 11600 cm^{-1}, respectively, the D-band at 16600 cm^{-1}, and F-band (intramolecular transition of $TCNQ^{\bullet-}$) at 27600 cm^{-1},[33] while the significant absorption bands were observed at 30000–31000 cm^{-1} in 1,3-DAP·H^+ salts, and 20000–23000 and 36000–37000 cm^{-1} in 1,6-DAP·H^+ salts, respectively. These spectral features of CT salts indicate that the TCNQ molecules in these CT salts are completely ionized radical anions. The differences in the electronic spectra from $K^+TCNQ^{\bullet-}$ represent the increment of the intensity of the C-band and the lower shift of the B-band in (**6a**·H^+)-($TCNQ^{\bullet-}$)$(H_2O)_{0.25}$ and (**7b**)(**7b**·H^+)($TCNQ^{\bullet-}$)$(H_2O)_2$ salts. These differences seem to be caused by the changes of the molecular packing of $TCNQ^{\bullet-}$ molecules in these CT salts. The cationic states of these DAP moieties were evaluated to be a protonated cation, DAP·H^+, by comparing their C=C and C=N stretching frequencies in the IR spectra[17f,18c] to those of neutral DAP and protonated DAP·H^+. Figure 12 shows the IR spectra of neutral species, HBr salts and $TCNQ^{\bullet-}$ salts of **5a**, **6a**, and **7a** in the frequency range 1450–1700 cm^{-1}. In the case of **5a**, the C=C and C=N stretching frequencies were observed at 1639, 1609, and 1590 cm^{-1} for neutral species and 1664 and 1629 cm^{-1} for the HBr salt. Thus, the $TCNQ^{\bullet-}$ salt of **5a**, which exhibited the frequencies at 1667 and 1638 cm^{-1}, was assigned to be (**5a**·H^+)($TCNQ^{\bullet-}$)$(H_2O)_{0.4}$ (Fig. 12a). The absorption bands observed at around 1505 and 1580 cm^{-1} are assigned to the B_{2u} and B_{1u} modes of C=C stretching of $TCNQ^{\bullet-}$ moieties, respectively.[35] The other protonated DAPs salts with $TCNQ^{\bullet-}$, except for the 2:1 salt of **7b** and $TCNQ^{\bullet-}$, showed similar behavior to that of the **5a** system in the IR spectra and were determined to be the 1:1 salt of DAP·H^+ and $TCNQ^{\bullet-}$ (Fig. 12). The 2:1 salt of **7b** and $TCNQ^{\bullet-}$ exhibited three C=C and C=N stretching frequencies of the DAP moiety. The bands at 1606 and 1543 cm^{-1} were assigned to the C=C and C=N stretching frequencies of protonated **7b**·H^+ and neutral **7b**, respectively. The band at 1637 cm^{-1} can be assigned to be those of both **7b** and **7b**·H^+ (Fig. 12c). These facts indicate that the cationic state of the **7b** moiety in this complex was the mixed state of the neutral and protonated cation.

Crystal Structure of $TCNQ^{\bullet-}$ Salt of 2-*t*-Butyl-1,3-DAP·H^+ [(5c·H^+)($TCNQ^{\bullet-}$)$(H_2O)_{0.5}$]: This salt was composed of **5c**·H^+, $TCNQ^{\bullet-}$, and water molecules (Fig. 13a). The water molecule was disordered over five positions and refined with isotropic thermal parameters. Similar to those in (**5c**·H^+)(Br^-) and (**5c**·H^+)(BF_4^-), intramolecular C1–N1 and C1–N2 bond lengths showed no notable bond alternation (Table 4). This result implies delocalization of the plus charge around the N1–C1–N2 bond and formation of H-bonding interactions in this salt. The ionicity of the TCNQ molecule was deduced as −1 from the bond lengths, and assigned to be a complete radical anion (Table 7).[36] These results coincided with the ionicity from the spectral analyses. Both **5c**·H^+ and $TCNQ^{\bullet-}$ molecules formed π-stacking dimers with the slipped head-to-tail fashion and the nearly eclipsed one, respectively (Figs. 13b and 13c). These dimers alternately stacked to form a one-dimensional column along the [011] direction in a DDAA manner (Figs. 13d and 13e). The face-to-face distances in the π-stacking column were 3.50 Å for the **5c**·H^+ dimer, 3.24 Å for the $TCNQ^{\bullet-}$ dimer, and ca. 3.7 Å for the interdimer stack of **5c**·H^+–$TCNQ^{\bullet-}$. Interestingly, two N–H groups of **5c**·H^+ formed intermolecular H-bonds with C≡N groups in the TCNQ molecule, resulting in the formation of a cyclic tetramer composed of two **5c**·H^+ and two $TCNQ^{\bullet-}$ molecules (Fig. 13f). The H-bonding lengths were 3.01 Å for N1···N6 and 3.06 Å for N2···N3. This H-bonding interaction connected the π-stacking columns, and these interactions formed the three-dimensional network of this crystal (Fig. 13g).

Crystal Structure of 2:1 TCNQ Salt of 7,9-Dichloro-2-methyl-5-phenyl-1,6-DAP·H^+ [(7b)(7b·H^+)($TCNQ^{\bullet-}$)-$(H_2O)_2$]: This crystal consisted of the crystallographically independent one **7b**, $TCNQ^{\bullet-}$, and H_2O molecules (Fig. 14a). The water molecule was disordered and refined with isotropic thermal parameters. The TCNQ molecule was located on the center of inversion and showed a planar structure. The formal charge of the TCNQ molecule was estimated to be −1 from the intramolecular C–C bond lengths (Table 7).[36] The C=C and C=N stretching frequencies in the IR spectra indicated that this salt contained both neutral and protonated species of **7b** (Fig. 12c). These results show that the component ratio

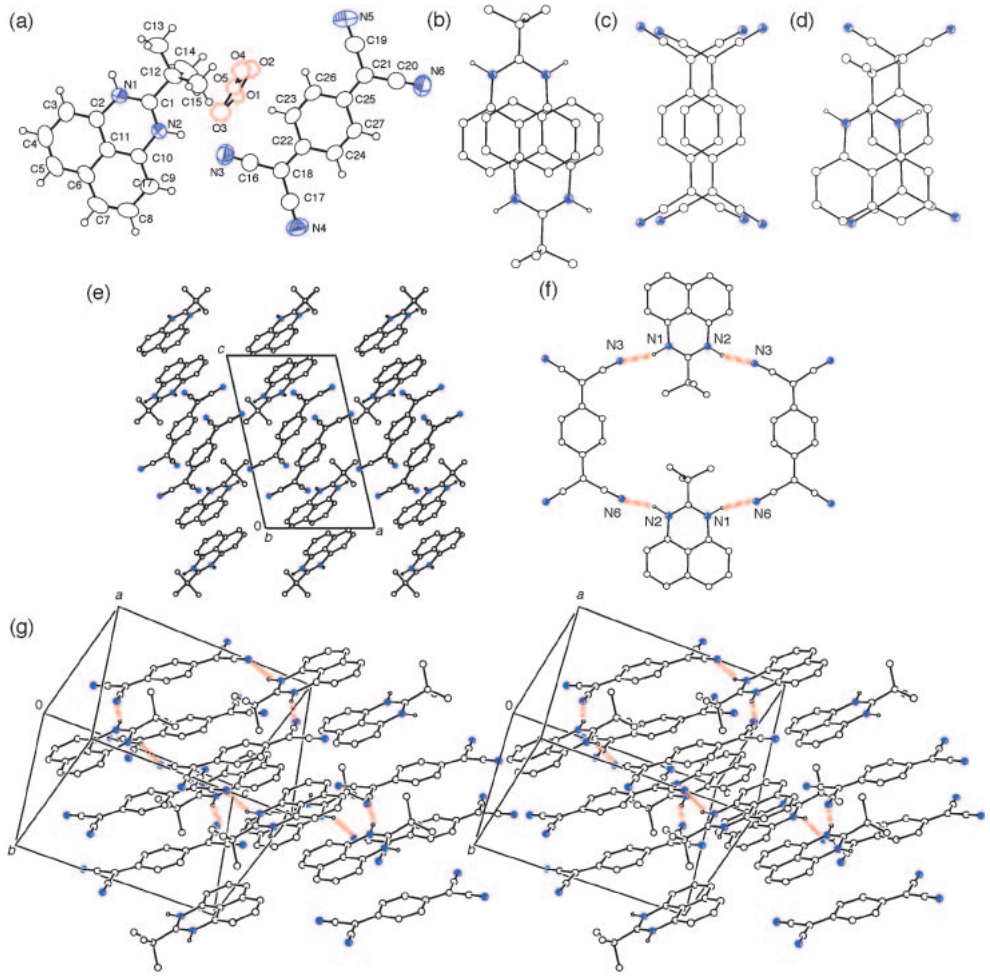

Fig. 13. Crystal structure of (**5c**·H^+)($TCNQ^{\bullet-}$)$(H_2O)_{0.5}$. Molecular structure and atomic numbering scheme (a). Overlap modes in π-stacking columns of **5c**·H^+–**5c**·H^+ (b), $TCNQ^{\bullet-}$–$TCNQ^{\bullet-}$ (c), and **5c**·H^+–$TCNQ^{\bullet-}$ (d). DAAD stacking column along the [011] direction (e). Cyclic tetramer formed by N–H···N≡C H-bonds (f). Stereoview of the crystal packing showing the π-stacking and H-bonded structures (g).

Table 7. C–C Bond Lengths of TCNQ Moieties in (**5c**·H^+)($TCNQ^{\bullet-}$)$(H_2O)_{0.5}$, (**7b**)(**7b**·H^+)($TCNQ^{\bullet-}$)$(H_2O)_2$, Neutral $TCNQ^0$, and Completely Ionic $TCNQ^{\bullet-}$

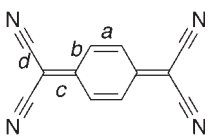

	a/Å	b/Å	c/Å	d/Å
(**5c**·H^+)($TCNQ^{\bullet-}$)$(H_2O)_{0.5}$	1.355(3), 1.355(3)	1.419(3), 1.418(3)	1.423(3), 1.418(3)	1.431(3), 1.397(3)
		1.416(3), 1.431(3)		1.407(3), 1.417(4)
(**7b**)(**7b**·H^+)($TCNQ^{\bullet-}$)$(H_2O)_2$	1.367(6)	1.405(6), 1.419(6)	1.425(6)	1.417(6), 1.425(6)
$TCNQ^{0}$ [a]	1.346	1.448	1.374	1.441
$TCNQ^{\bullet-}$ [b]	1.373	1.426	1.420	1.416

a) Ref. 36a. b) Ref. 36b.

in this salt was determined to be **7b**:**7b**·H^+:$TCNQ^{\bullet-}$ = 1:1:1, and that the **7b** molecule in this crystal structure possessed an excess proton (H2) with half occupancy on the N2–H group. The DAP skeleton of the **7b** moiety was nearly planar, and the phenyl group was found to be inclined by 28.9° from the DAP skeleton. Similar to the intramolecular bond lengths of (**7b**)(MeOH) and (**6e**·H^+)(Br^-), which exhibited strong H-bonding interactions, the DAP skeleton of this salt showed no noticeable bond alternation (Table 5). The N–H groups in the **7b** neighboring the methyl group (N1) formed a H-bond with the C≡N group in TCNQ with a N1···N3 distance of 3.08 Å. This H-bonding interaction resulted in the formation of the trimeric pair of **7b**–TCNQ–**7b**, which contained one excess proton (Fig. 14b). Both **7b** and TCNQ molecules were

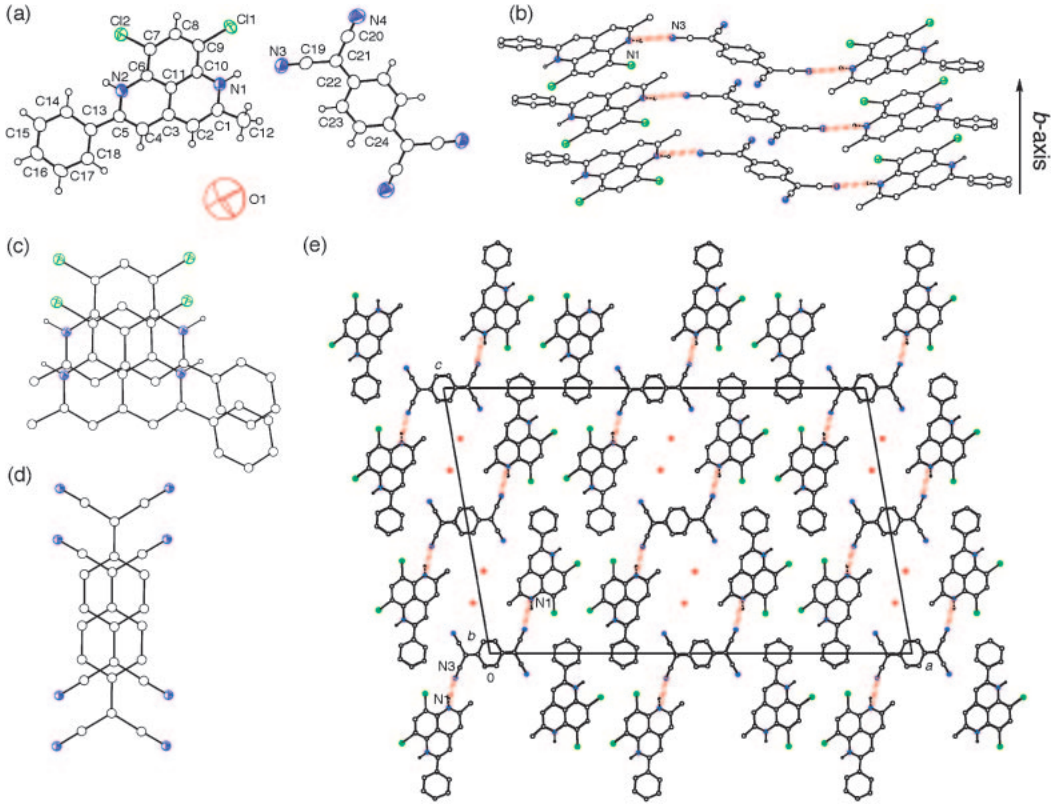

Fig. 14. Crystal structure of (**7b**)(**7b**·H^+)($TCNQ^{\bullet -}$)$(H_2O)_2$. Molecular structure and atomic numbering scheme (a). Segregated stacking column of **7b** and TCNQ connected by N–H···C≡N H-bonds (b). Overlap mode in π-stacking columns of **7b** (c) and TCNQ (d). Crystal packing viewed along the *b*-axis illustrating the **7b**–TCNQ–**7b** triad formed by the N–H···C≡N H-bond (e).

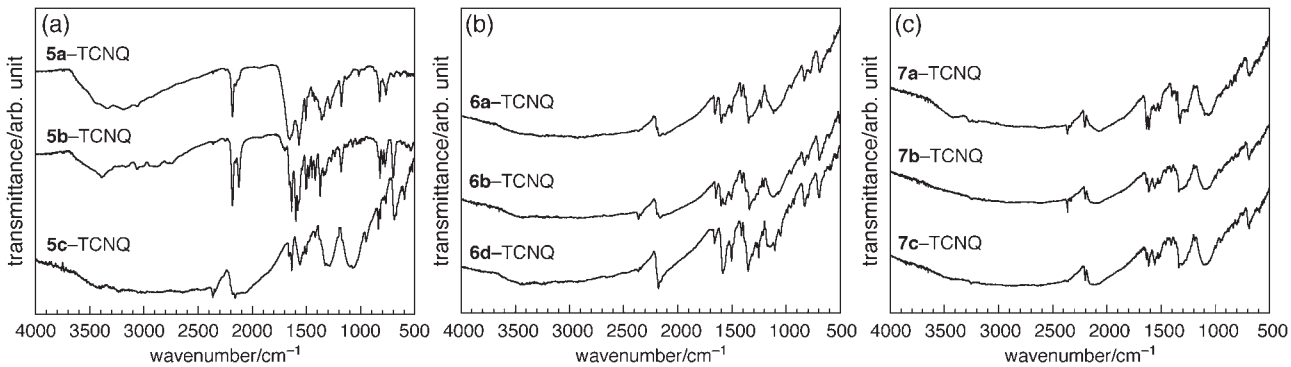

Fig. 15. IR spectra in KBr pellets of DAP–TCNQ complexes: **5a**–**5c** (a), **6a**, **6b**, **6d** (b), and **7a**–**7c** (c).

arranged in uniform and segregated stacks along the *b*-axis with face-to-face distances of 3.37 Å for **7b** and 3.21 Å for TCNQ (Figs. 14b–14d). These π-stacking and H-bonding interactions formed a channel structure along the *b*-axis, and this channel was filled with two water molecules (Fig. 14e).

CT Complexes Composed of DAPs with TCNQ. Figures 15 and 16 display IR and electronic spectra of the TCNQ complexes with **5a**–**5c**, **6a**, **6b**, **6d**, and **7a**–**7c**. Table 8 summarizes the molecular ratios of these CT complexes elucidated from elemental analysis, nitrile stretching frequency, ionicity of the TCNQ moiety by Chappell's method,[34] and frequency of CT bands.[33] However, estimation of the ionicity of the TCNQ molecule remains ambiguous because it often gives inaccurate values for an ionicity larger than ≈0.5,[37] and the nitrile stretching frequency is sensitive to environmental perturbation such as H-bonding formation. Although there was no direct information about the ionicity of the DAP moiety, the instability of its radical cation species due to the highly acidic N–H groups as shown in the electrochemical measurements and some resemblance in C=C and C=N stretching frequency in IR spectra imply that the DAP moiety in these CT complexes existed as a protonated cation. Thus, the ionicity of the DAP moiety in each of these complexes was estimated from their IR spectra in the range of 1450–1700 cm^{-1} by comparison with neutral and HBr salts of DAPs (Fig. 17). The room temperature electrical conductivity (σ_{rt}) of DAPs–TCNQ complexes on compressed pellets were 10^{-2}–10^{-1} S cm^{-1} with low activation energies (E_a, 40–78 meV), which were compa-

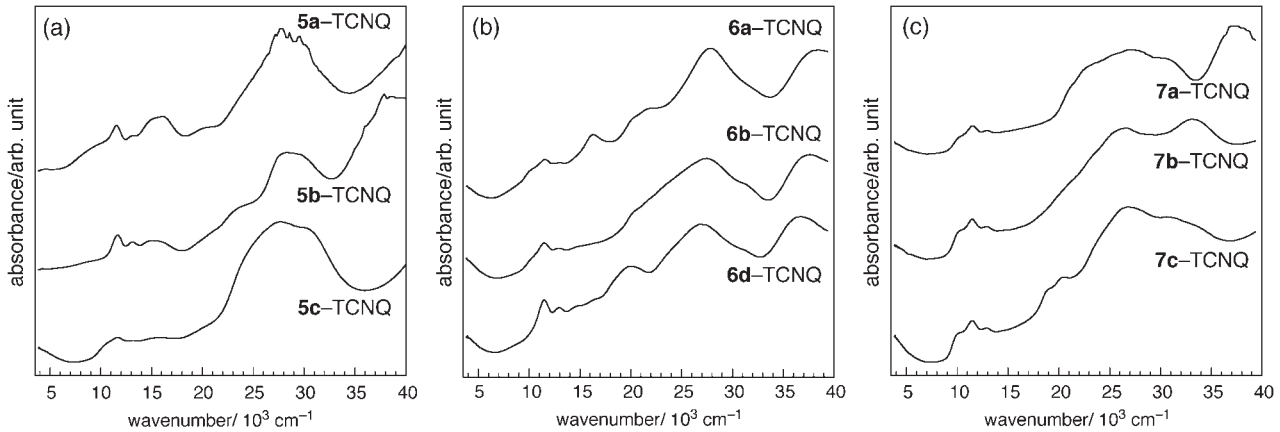

Fig. 16. Electronic spectra in KBr pellets of DAP–TCNQ complexes: **5a**–**5c** (a), **6a**, **6b**, **6d** (b), and **7a**–**7c** (c).

Table 8. Physical Properties of CT Complexes with TCNQ Prepared by the Mixing Method

	D:A[a]	ν_{CN}[b]/cm^{-1}	Ionicity of TCNQ[c]	A-band[b] /10^3 cm^{-1}	B-band[b] /10^3 cm^{-1}	C-band[b] /10^3 cm^{-1}	D-band[b] /10^3 cm^{-1}	F-band[b] /10^3 cm^{-1}	σ_{rt}[d]/S cm^{-1}	E_a/meV
5a	3:2	2182	≈1	—[e]	8.7sh	11.6	16.1	27.9	—[f]	—[f]
5b	3:2	2182	≈1	—[e]	—[e]	11.7	15.0	28.4	—[f]	—[f]
5c	1:2	2200	0.61	2.9	—[e]	11.7	15.8	27.6	1.6×10^{-1}	67
6a	1:1	2197	0.68	2.9	10.0sh	11.6	16.4	28.1	2.9×10^{-2}	72
6b	1:1	2196	0.70	3.0	9.9sh	11.5	16.5	27.8	2.9×10^{-2}	78
6d	1:1	2199	0.64	3.1	—[e]	11.5	15.1, 16.8	27.2	6.3×10^{-5}	145
7a	3:1	2203	0.55	2.6	10.0sh	11.5	—[e]	27.2	4.3×10^{-2}	40
7b	5:6	2202	0.57	2.8	10.5	11.5	—[e]	27.0	1.9×10^{-2}	58
7c	2:3	2200	0.61	2.8	9.8sh	11.5	—[e]	27.0	1.6×10^{-1}	52

a) Molar ratio was estimated by the elemental analysis. b) IR and electronic spectra were measured in KBr pellets. c) The ionicity of TCNQ was estimated by the C≡N stretching frequency of the IR spectrum on the basis of Chappell's method.[34,37] d) Electrical conductivity was measured by the four-probe or two-probe method on a compressed pellet. e) The peak was not observed. f) Not measured.

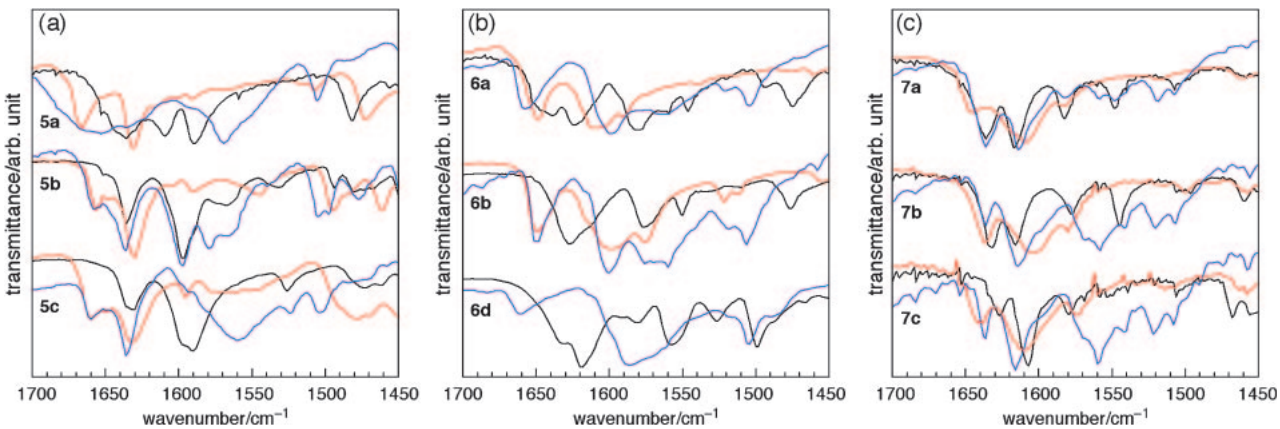

Fig. 17. IR spectra of neutral species (black line), HBr salts (red line), and TCNQ complexes (blue line) of DAPs **5a**–**5c** (a), **6a**, **6b**, **6d** (b), and **7a**–**7c** (c) in the frequency range 1450–1700 cm^{-1} measured by KBr pellet.

rable to that of the TCNQ complex of the 1,9-dithiophenalenyl systems **2** (≈10^{-2} S cm^{-1}) reported by Haddon and Wudl.[6]

TCNQ Complexes of 1,3-DAPs 5a–5c: **5a**– and **5b**–TCNQ showed the nitrile (2182 cm^{-1}) stretching mode of the TCNQ molecule at lower frequency. Both of the absorption bands in the electronic spectra of these complexes resembled those of $K^+TCNQ^{\bullet-}$ (Fig. 16a). These results indicate that the TCNQ moieties in **5a**– and **5b**–TCNQ were completely anionic species. The C=C and C=N absorption bands of the DAP moiety at 1597 and 1658 cm^{-1} in **5b**–TCNQ overlapped with those at 1598 cm^{-1} in neutral **5b** and at 1657 cm^{-1} in (**5b**·H^+)(Br^-), respectively. Considering the ionic state of the TCNQ molecule, these observations indicated that the **5b**–TCNQ complex was composed of neutral **5b**, cationic **5b**·H^+, and $TCNQ^{\bullet-}$, whereas the **5a**–TCNQ complex showed broad bands at the C=C and C=N absorption range, and assignment

of the ionicity of **5a** was difficult. Considering the 3:2 molecular ratio, the DAP moiety in **5a**–TCNQ was assigned to be a mixture of neutral **5a** and cationic **5a**·H^+, similar to **5b**–TCNQ. From these results, the compositions of these complexes can be deduced as (**5a**)(**5a**·H^+)$_2$(TCNQ$^{\bullet-}$)$_2$ and (**5b**)(**5b**·H^+)$_2$(TCNQ$^{\bullet-}$)$_2$. In the case of **5c**–TCNQ, the ionicity of the TCNQ moiety was estimated to be 0.61 by the nitrile stretching frequency.[34] Furthermore, this complex exhibited low-energy absorption around 3000 cm^{-1} (A-band), which was assigned to be an intermolecular CT transition from TCNQ$^{\bullet-}$ to TCNQ^0 (Fig. 16a).[33] This spectral feature indicates the partially ionic state of the TCNQ moiety in **5c**–TCNQ. The C=C and C=N stretching frequencies at 1660 cm^{-1} in **5c**–TCNQ were similar to that of protonated **5c**·H^+, 1658 cm^{-1}, rather than that of neutral **5c**, 1630 cm^{-1} (Fig. 17a). Thus, the electronic structure of the **5c** moiety in this complex was deduced to be cationic **5c**·H^+. Considering the molecular ratio also, the composition of this complex can be deduced as (**5c**·H^+)(TCNQ$^{0.5-}$)$_2$. The difference between the ionicities of the TCNQ moiety of 0.61 from the nitrile stretching frequency and of 0.5 from the molecular ratio might be induced by an environmental perturbation. Measurement of electrical conductivity for **5c**–TCNQ showed a relatively high σ_{rt} of 1.6×10^{-1} S cm^{-1} with semiconductive behavior (E_a = 67 meV).

TCNQ Complexes of 7-Substituted 1,6-DAPs 6a, 6b, and 6d: The molecular ratios of all **6a**–, **6b**–, and **6d**–TCNQ complexes were estimated to be 1:1 from elemental analyses. The C≡N stretching frequencies indicate the ionized state of the TCNQ moiety in these complexes.[34] The lower energy absorption bands around 3000 cm^{-1} suggested that these complexes were partial CT complexes (Fig. 16b).[33] The protonated state of the **6a**, **6b**, and **6d** moieties could be rationalized by considering the C=C and C=N stretching frequencies at 1657 cm^{-1} in **6a**–TCNQ, 1648 cm^{-1} in **6b**–TCNQ, and 1661 cm^{-1} in **6d**–TCNQ in IR spectra (Fig. 17b). The HBr salt of **6d** was not obtained due to the instability of **6d** under highly acidic conditions, and the ionicity in the TCNQ complex was deduced according to the pattern of C=C and C=N stretching bands of the HBr salts of **6a** and **6b**. σ_{rt} values for **6a**–TCNQ and **6b**–TCNQ were 2.9×10^{-2} S cm^{-1}, with E_a values of 72 and 78 meV, respectively. The σ_{rt} value of **6d**–TCNQ was lower ($\sigma_{rt} = 6.3 \times 10^{-5}$ S cm^{-1} and E_a = 145 meV) than those of **6a**– and **6b**–TCNQ complexes.

TCNQ Complexes of Tetrasubstituted 1,6-DAPs 7a–7c: In spite of the sterically hindered environment around the DAP skeleton, the tetrasubstituted 1,6-DAPs **7a**–**7c** also form CT complexes with TCNQ. The C≡N stretching frequency (2000–2003 cm^{-1}) showed the ionized state of the TCNQ moieties.[34] The nature of the partial CT in these complexes were deduced as low-energy CT bands at around 3000 cm^{-1} (Fig. 16c).[33] The C=C and C=N stretching frequencies in the IR spectra of **7a**– and **7b**–TCNQ complexes were observed between those of neutral and protonated species, and implied that these complexes contained both neutral and cationic DAPs. On the other hand, a slightly higher frequency shift of C=C and C=N stretching frequencies in the **7c**–TCNQ complex than neutral **7c** implied that the electronic structures of the 1,6-DAP moieties were a completely cationic state (Fig. 17c). These complexes showed a high σ_{rt} value of 10^{-2}–10^{-1} S cm^{-1} with lower E_a values (40–58 meV).

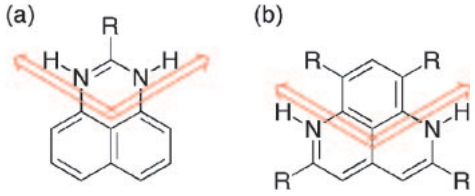

Fig. 18. Schematic drawing of the directionality of the H-bonding interactions of protonated 1,3- and 1,6-DAP systems, (a) and (b), respectively.

Discussion

CT Complex Formation. 1,3- and 1,6-DAP systems showed a tendency to form a partial CT complex with TCNQ. The 1,3-DAP derivatives **5** formed ionic and partial CT complexes in spite of their poor electron-donating abilities (Tables 1 and 8). As for the 1,6-DAP derivative, the tendency to form a partial CT complex was more remarkable. Although some of the 1,6-DAP derivatives **6** and **7** possessed a stronger or weaker electron-donating ability, their CT complexes showed the partial CT state and exhibited relatively high electrical conductivity (Tables 1 and 8). The origin of these intriguing tendencies has not been clarified; however, extended π-conjugation of the phenalenyl systems[2] and/or electronic modulation[22b,23] induced by H-bonding ability might play a key role in the formation of partial CT complexes.

In the crystal structures of protonated 1,3-DAP salts, 1,3-DAP molecules showed an angular bridging mode of H-bonds parallel or nearly parallel to the molecular plane, which constructed the well defined H-bonded structures (Fig. 18a). The HBr salts of 1,3-DAP, (**5b**·H^+)(Br^-) and (**5c**·H^+)(Br^-) constructed one-dimensional tape structures by H-bonds across counter anions parallel to the molecular plane (Figs. 6b, 7b, and 7c). In (**5c**·H^+)(BF_4^-) salt, the N(2)–H···F(4) H-bond was not parallel to the molecular plane due to the steric repulsion between the *t*-butyl group and BF_4^- anion, resulting in the formation of a zigzag one-dimensional chain (Fig. 8f). In the TCNQ salt of protonated **5c**, (**5c**·H^+)(TCNQ$^{\bullet-}$)(H_2O)$_{0.5}$, both the **5c**·H^+ molecule and TCNQ formed the angular bridging mode of H-bonds to construct a cyclic tetramer unit (Fig. 13f).

In the 1,6-DAP system, it is expected that its H-bonding directionality is similar to that of 1,3-DAP (Fig. 18b). Actually, the **6e**·H^+ molecule in (**6e**·H^+)(Br^-) salt formed the angular bridging mode of H-bonds parallel to the molecular plane. However, steric repulsion between chlorine atoms and the small H-bonding angle of bromide anions constructed the two-fold screw H-bonded chain unlike the tape-like H-bonded chain seen in (**5b**·H^+)(Br^-) and (**5c**·H^+)(Br^-) salts (Fig. 9b). In the crystal structure of (**7b**)(MeOH), the steric hindrance of the phenyl group prevented the formation of H-bonding interaction parallel to the molecular plane. Thus, (**7b**)(MeOH) formed H-bond directing parallel to π-stacking, resulting in the formation of a H-bonded face-to-face dimer (Fig. 5b). In (**7b**)(**7b**·H^+)(TCNQ$^{\bullet-}$)(H_2O)$_2$, the N(1) atom formed H-bonding interaction with TCNQ, while the N(2) atom, which is next to the phenyl group, could not form an H-bond, leading to the formation of a closed D–A–D triad (Fig. 14e). These ob-

servations confirmed that the H-bonding interaction of 1,3- and 1,6-DAP systems played an important role in the control of the molecular aggregation, and that H-bonding structures can be easily controlled by the steric environment of substituents on the DAP systems and by the directionality of the H-bond of counter anions.

Conclusion

1,3- and 1,6-DAP systems, nitrogen analogues of a phenalenyl system, have been utilized as the electron-donor molecules of CT salts and complexes having H-bonded networks. Furthermore, the crystal structures of neutral and protonated salts of DAPs have been investigated in this work. The common structural feature of these neutral and protonated DAP systems is the formation of H-bonds through the N–H moieties and π-stacking dimeric or columnar structures. The formation of N–H···N≡C H-bonding observed in the crystal structure of the $TCNQ^{\bullet-}$ salt of protonated **5c** and **7b** is an important finding for further study to construct CT complexes with multiple H-bonded networks. The electronic states of the TCNQ moiety of the CT salts of protonated DAPs or the CT complex of DAPs varied from complete to partial ionic states. All of the TCNQ salts of protonated DAP gave completely ionic CT salts with a 1:1 molecular ratio. To the contrary, TCNQ complexes prepared by direct mixing of DAP and TCNQ, except for **5a**–TCNQ and **5b**–TCNQ, were partial CT complexes with high electrical conductivities (10^{-1}–10^{-2} S cm^{-1} at room temperature) with semiconductive behaviors. These results show the high potential of DAP systems as component molecular systems of CT complexes having well-defined structures by H-bonds and high electrical conductivity. These observations and properties of DAP systems stimulate further challenges on molecular design and control of directional H-bonds and the degree of CT interactions. X-ray crystal structure analyses for TCNQ complexes of DAPs are the first step for realizing our purpose directed toward the construction of H-bonded CT complexes with structurally and electronically modulated functionalities by H-bond such as proton- and electron-conducting supramolecular assemblies and cooperative proton-coupled electron-transferring systems.[20]

Experimental

Materials and Methods. All experiments with moisture- or air-sensitive compounds were performed in anhydrous solvents under an argon atmosphere in flame-dried glassware. Solvents were dried and distilled according to the standard procedures. The water molecules in these CT complexes came from atmospheric moisture under preparation. R_f values on TLC were recorded on E. Merck precoated (0.25 mm) silica gel 60 F_{254} plates. Silica gel 60 (100–200 mesh) was used for column chromatography. Preparative gel permeation chromatography (GPC) was performed on a Japan Analytical Industry LC-908 equipped with a JAIGEL 1H column and a LC-908 C60 equipped with a JAIGEL 2H-40 assembly with $CHCl_3$ as the eluant. Melting points were measured with a hot-stage apparatus and are uncorrected. Elemental analyses were performed at the Graduate School of Science, Osaka University. Infrared spectra were recorded on Perkin-Elmer FT 1640 IR and JASCO FT/IR-660 Plus spectrometers. Electronic spectra were measured by a Shimadzu UV-3100PC spectrometer. ^{1}H NMR spectra were obtained on a JEOL EX-270. EI-Mass spectra were taken at 70 eV by using a Shimadzu QP-5000 mass spectrometer. Cyclic voltammetric measurements were made with an ALS Electrochemical Analyzer Model 612A. Cyclic voltammograms were recorded with 3.0 mm diameter glassy plate carbon and Pt wire counter electrodes in dry DMF (obtained by distillation over CaH_2 under reduced pressure) containing 0.1 M *n*-Bu_4NBF_4 as the supporting electrolyte at room temperature. The experiments employed a $Ag/AgNO_3$ reference electrode by a semi-derivative method and the final results were calibrated with the ferrocene/ferrocenium couple. The direct current electrical-conductivity measurements were performed on the compressed powder by a conventional four-probe method using gold paint and gold wire. X-ray crystallographic measurements were made on a Rigaku AFC7R diffractometer or Rigaku Raxis-Rapid Imaging Plate with graphite monochromated Mo Kα radiation. The structures of **5c**, (**7b**)(MeOH), (**7b**)(**7b**·H^+)($TCNQ^{\bullet-}$)$(H_2O)_2$, (**5c**·H^+)(BF_4^-), and (**5c**·H^+)($TCNQ^{\bullet-}$)$(H_2O)_{0.5}$ were determined by a direct method using SHELXS-86[38] or SHELXS-97.[39] The structures of (**5b**·H^+)(Br^-), (**5c**·H^+)(Br^-), and (**6e**·H^+)(Br^-) were solved by heavy-atom Patterson methods (PATTY) and expanded using Fourier techniques (DIRDIF-94).[40] The least-square refinements were performed by full-matrix least squares on F for **5c**, (**5b**·H^+)(Br^-), (**5c**·H^+)(Br^-), and (**6e**·H^+)(Br^-), F^2 for (**7b**)(MeOH) and (**5c**·H^+)(BF_4^-), and on F^2 with SHELXL-97[41] for (**5c**·H^+)($TCNQ^{\bullet-}$)$(H_2O)_{0.5}$ and (**7b**)(**7b**·H^+)($TCNQ^{\bullet-}$)$(H_2O)_2$. All calculations were performed using the teXsan[42] crystallographic software package. All non-hydrogen atoms were refined anisotropically. Hydrogen atoms were refined isotropically, or were included without refinement. An empirical or symmetry-related absorption correction was applied for (**7b**)(MeOH), (**5b**·H^+)(Br^-), (**5c**·H^+)(Br^-), (**6e**·H^+)(Br^-), (**5c**·H^+)($TCNQ^{\bullet-}$)$(H_2O)_{0.5}$, and (**7b**)(**7b**·H^+)($TCNQ^{\bullet-}$)$(H_2O)_2$. Crystallographic data have been deposited with Cambridge Crystallographic Data Centre: Deposition numbers CCDC-297883–297890. Copies of the data can be obtained free of charge via http://www.ccdc.cam.ac.uk/conts/retrieving.html (or from the Cambridge Crystallographic Data Centre, 12, Union Road, Cambridge, CB2 1EZ, UK; Fax: +44 1223 336033; e-mail: deposit@ccdc.cam.ac.uk).

7,9-Dichloro-2,5-dimethyl-1,6-DAP (7a). Typical Procedure for the Synthesis of 7,9-Dichloro-2-methyl-5-R-1,6-DAPs. To a solution of diisopropylamine (0.59 mL, 4.14 mmol) in THF (5 mL) was added butyllithium (1.6 M hexane solution, 2.60 mL, 4.14 mmol) at −78 °C, and the solution was stirred at this temperature for 15 min. **8b** (500 mg, 2.07 mmol) was added in THF (15 mL) to this mixture and the reaction mixture was gradually warmed up to room temperature over 1 h. Ethyl acetate (0.30 mL, 3.11 mmol) was added to this mixture and stirred at room temperature for 4 h. The resulting mixture was poured into a saturated NH_4Cl aqueous solution (20 mL) and extracted with ethyl acetate (20 mL). The organic extract was washed with a saturated NaCl aqueous solution (20 mL) and dried over Na_2SO_4, then filtered, and concentrated under reduced pressure. The residual oil was diluted with EtOH (3 mL) and the resulting powder was washed with EtOH (10 mL) to give **7a** (94.4 mg, 17%) as a yellowish green powder: mp 230–231 °C (dec); TLC R_f 0.36 (1:1 benzene/ethyl acetate); ^{1}H NMR (270 MHz, $CDCl_3$) δ 2.21 (s, 3H), 2.54 (s, 3H), 5.72 (s, 1H), 6.40 (s, 1H), 7.21 (brs, 1H), 7.54 (s, 1H); IR (KBr) 3415, 1636, 1617, 1583, 1548 cm^{-1}; IR (tetrachloroethylene) 3419, 1644, 1616, 1584 cm^{-1}; UV (MeOH) 416, 384, 368, 323, 259 nm; EI-MS m/z 264 (M^+, 100%); Anal. Calcd for ($C_{13}H_{10}Cl_2N_2$)$(H_2O)_{0.25}$: C, 57.91; H, 3.92; N, 10.39%. Found: C, 57.91; H, 3.81; N, 10.37%.

7,9-Dichloro-2-methyl-5-phenyl-1,6-DAP (7b): 18% yield; bright yellow solid: mp 212–214 °C; TLC R_f 0.39 (2:1 hexane/ethyl acetate); ^{1}H NMR (270 MHz, $CDCl_3$) δ 2.32 (s, 3H), 5.99 (s, 1H), 6.80 (s, 1H), 7.42–7.54 (m, 4H), 7.59 (s, 1H), 8.01 (s, 2H); IR (KBr) 3405, 1632, 1616, 1577, 1545 cm^{-1}; IR (tetrachloroethylene) 3418, 1639, 1618, 1583, 1548 cm^{-1}; UV (MeOH) 435, 384, 332 nm; EI-MS m/z 326 (M^+, 100%); Anal. Calcd for $C_{18}H_{12}Cl_2N_2$: C, 66.07; H, 3.70; N, 8.56%. Found: C, 66.10; H, 3.56; N, 8.76%. Recrystallization from MeOH gave single crystals of (**7b**)(MeOH) suitable for X-ray structural analysis as yellow blocks.

7,9-Dichloro-2-methyl-5-(2′-pyridyl)-1,6-DAP (7c): 41% yield; vivid reddish orange solid: mp 220–222 °C; TLC R_f 0.21 (1:1 hexane/ethyl acetate); ^{1}H NMR (270 MHz, $CDCl_3$) δ 2.54 (s, 3H), 6.42 (s, 1H), 6.77 (s, 1H), 7.38–7.44 (m, 1H), 7.60 (s, 1H), 7.80–7.90 (m, 1H), 8.02 (s, 1H), 8.68 (d, 1H, $J = 5.0$ Hz), 9.41 (s, 1H); IR (KBr) 3316, 1627, 1607, 1579, 1552 cm^{-1}; IR (tetrachloroethylene) 3418, 3341, 1609, 1580 cm^{-1}; UV (MeOH) 451, 383, 339 nm; EI-MS m/z 327 (M^+, 100); Anal. Calcd for $C_{17}H_{11}Cl_2N_3$: C, 62.21; H, 3.38; N, 12.80%. Found: C, 61.99; H, 3.30; N, 12.74%.

1,3-DAP·H$^+$ Bromide [(5a·H$^+$)(Br$^-$)]. Typical Procedure for the Preparation of Protonated Salts of DAPs. The 1,3-DAP (**5a**) (74.2 mg, 0.44 mmol) was placed in a 30-mL round-bottomed flask and dissolved with MeOH (7 mL). A 47% HBr aqueous solution (0.10 mL, 0.86 mmol) was added to the mixture at room temperature. The reaction mixture was stirred at room temperature for 1 h, and left standing at −10 °C. The resulting powder was collected by filtration, and washed with MeOH (3 mL) and Et_2O (3 mL) to give the protonated salt (45.7 mg) as a bright greenish yellow powder. mp 260–263 °C (dec); IR (KBr) 3200–2600, 1664, 1629 cm^{-1}; UV (KBr) 324, 226 nm; Anal. Calcd for $C_{12}H_9BrN_2$: C, 53.04; H, 3.64; N, 11.25%. Found: C, 52.96; H, 3.50; N, 11.26%.

2-Phenyl-1,3-DAP·H$^+$ Bromide [(5b·H$^+$)(Br$^-$)]: Vivid orange crystal: mp 262–265 °C (dec); IR (KBr) 3094, 3047, 3000–2600, 1657, 1630 cm^{-1}; UV (KBr) 332, 220 nm; Anal. Calcd for $C_{17}H_{13}BrN_2$: C, 62.79; H, 4.03; N, 8.61%. Found: C, 62.67; H, 3.84; N, 8.60%. Recrystallization from EtOH gave single crystals of (**5b**·H$^+$)(Br$^-$) suitable for X-ray structural analysis as vivid orange platelets.

2-*t*-Butyl-1,3-DAP·H$^+$ Bromide [(5c·H$^+$)(Br$^-$)]: Bright yellow crystal: mp 293–298 °C (dec); IR (KBr) 3300–2600, 1658, 1630 cm^{-1}; UV (KBr) 322, 226 nm; Anal. Calcd for $C_{15}H_{17}BrN_2$: C, 59.03; H, 5.61; N, 9.18%. Found: C, 59.00; H, 5.53; N, 9.18%. Recrystallization from EtOH gave single crystals of (**5c**·H$^+$)(Br$^-$) suitable for X-ray structural analysis as bright yellow blocks.

2-*t*-Butyl-1,3-DAP·H$^+$ Tetrafluoroborate [(5c·H$^+$)(BF_4^-)]: Bright greenish yellow crystal: mp 279–282 °C (dec); IR (KBr) 3600–2800, 1663, 1636, 1096 cm^{-1}; Anal. Calcd for $C_{15}H_{17}BF_4N_2$: C, 59.03; H, 5.61; N, 9.18%. Found: C, 59.00; H, 5.53; N, 9.18%. Vapor diffusion with *i*-Pr_2O/EtOH gave single crystals of (**5c**·H$^+$)(BF_4^-) suitable for X-ray structural analysis as bright yellow blocks.

1,6-DAP·H$^+$ Bromide [(6a·H$^+$)(Br$^-$)]: Brownish olive solid: mp 279–284 °C (dec); IR (KBr) 3200–2700, 1651, 1613, 1592 cm^{-1}; UV (KBr) 490, 460, 352, 266, 220 nm; Anal. Calcd for $(C_{11}H_9BrN_2)(C_2H_6O)_{0.15}$: C, 53.01; H, 3.90; N, 10.94%. Found: C, 53.17; H, 3.77; N, 10.73%.

7-Bromo-1,6-DAP·H$^+$ Bromide [(6b·H$^+$)(Br$^-$)]: Vivid yellowish orange powder: mp 263–269 °C (dec); IR (KBr) 3200–2600, 1647, 1597, 1573 cm^{-1}; UV (KBr) 458, 354, 268, 218 nm; Anal. Calcd for $C_{11}H_8Br_2N_2$: C, 40.28; H, 2.46; N, 8.54%. Found: C, 40.23; H, 2.40; N, 8.46%.

7-Iodo-1,6-DAP·H$^+$ Bromide [(6c·H$^+$)(Br$^-$)]: Vivid yellowish orange powder: mp 263–269 °C (dec); IR (KBr) 3200–2600, 1644, 1597 cm^{-1}; UV (KBr) 472, 360, 260 nm; Anal. Calcd for $(C_{11}H_8BrIN_2)(H_2O)$: C, 33.62; H, 2.56; N, 7.13%. Found: C, 33.24; H, 2.21; N, 7.05%.

2,5-Dichloro-1,6-DAP·H$^+$ Bromide [(6e·H$^+$)(Br$^-$)]: Dark brown crystal: mp 270–274 °C (dec); IR (KBr) 3000–2500, 1648, 1594, 1572 cm^{-1}; Anal. Calcd for $C_{11}H_7BrCl_2N$: C, 41.55; H, 2.22; N, 8.81%. Found: C, 41.90; H, 2.30; N, 8.58%. Recrystallization from EtOH gave single crystals of (**6e**·H$^+$)(Br$^-$) suitable for X-ray structural analysis as deep reddish orange blocks.

7,9-Dichloro-2,5-dimethyl-1,6-DAP·H$^+$ Bromide [(7a·H$^+$)(Br$^-$)]: Olive powder: mp 242–244 °C (dec); IR (KBr) 3500–2600, 1645, 1607, 1584 cm^{-1}; UV (KBr) 436, 357, 307, 267, 220 nm; Anal. Calcd for $(C_{13}H_{11}BrCl_2N_2)(H_2O)_{0.4}$: C, 44.20; H, 3.37; N, 7.93%. Found: C, 44.10; H, 3.31; N, 7.93%.

7,9-Dichloro-2-methyl-5-phenyl-1,6-DAP·H$^+$ Bromide [(7b·H$^+$)(Br$^-$)]: Orange powder: mp 248–251 °C (dec); IR (KBr) 3500–3200, 3200–2500, 1635, 1604, 1578 cm^{-1}; Anal. Calcd for $(C_{18}H_{13}BrCl_2N_2)(H_2O)_{0.8}$: C, 51.17; H, 3.48; N, 6.63%. Found: C, 51.18; H, 3.70; N, 6.34%.

7,9-Dichloro-2-methyl-5-(2′-pyridyl)-1,6-DAP·H$^+$ Bromide [(7c·H)(Br$^-$)]: Vivid red powder: mp 247–249 °C (dec); IR (KBr) 3500–3200, 3200–2500, 1636, 1608, 1573 cm^{-1}; Anal. Calcd for $(C_{17}H_{12}BrCl_2N_3)(H_2O)_{1.5}$: C, 46.82; H, 3.47; N, 9.63%. Found: C, 46.64; H, 3.35; N, 9.44%.

2-*t*-Butyl-1,3-DAP·H$^+$–TCNQ$^{\bullet-}$ Salt [(5c·H$^+$)(TCNQ$^{\bullet-}$)-(H_2O)$_{0.5}$]. Typical Procedure for the Preparation of TCNQ Salts of Protonated DAPs. Diazaphenalenium salt (**5c**·H$^+$)(Br$^-$) (17.7 mg, 0.06 mmol) was placed in a 30-mL round-bottomed flask and dissolved with EtOH (2.5 mL) at 48 °C. LiTCNQ (12.2 mg, 0.06 mmol) in EtOH (1.5 mL) was added to the mixture. After being stirred at the same temperature for 1 min, the mixture was left standing at room temperature for 12 h. The resulting powder was collected by filtration and washed with EtOH (2 mL) to give the TCNQ salt (14.1 mg) as a dark grayish purple microcrystalline. Single crystals suitable for X-ray structural analysis were obtained by concentration of the solution in a 150:1 mixture of acetone–EtOH as black blocks: mp 187–190 °C (dec); IR (KBr) 3100–2800, 2187, 2157, 1660, 1634, 1582, 1504 cm^{-1}; UV (KBr) 1030(sh), 852, 662, 372, 326, 222 nm; Anal. Calcd for $(C_{15}H_{17}N_2)(C_{12}H_4N_4)(H_2O)_{0.5}$: C, 73.95; H, 5.06; N, 19.16%. Found: C, 74.16; H, 5.06; N, 18.85%.

1,3-DAP·H$^+$–TCNQ$^{\bullet-}$ Salt [(5a·H$^+$)(TCNQ$^{\bullet-}$)]: Dark purplish blue powder: mp 178–181 °C (dec); IR (KBr) 3200–2600, 2191, 2178, 2154, 1667, 1638, 1583, 1508 cm^{-1}; UV (KBr) 874, 604, 354, 224 nm; Anal. Calcd for $(C_{11}H_9N_2)(C_{12}H_4N_4)(H_2O)_{0.4}$: C, 72.58; H, 3.65; N, 22.08%. Found: C, 72.99; H, 3.51; N, 21.70%.

2-Phenyl-1,3-DAP·H$^+$–TCNQ$^{\bullet-}$ Salt [(5b·H$^+$)(TCNQ$^{\bullet-}$)]: Dark grayish violet powder: mp 186–189 °C (dec); IR (KBr) 3200–2600, 2196, 2184, 2168, 1647, 1581, 1506 cm^{-1}; UV (KBr) 1028, 864, 646, 370, 220 nm; Anal. Calcd for $(C_{17}H_{13}N_2)(C_{12}H_4N_4)(H_2O)_{0.25}$: C, 76.72; H, 3.89; N, 18.51%. Found: C, 76.72; H, 3.69; N, 18.33%.

1,6-DAP·H$^+$–TCNQ$^{\bullet-}$ Salt [(6a·H$^+$)(TCNQ$^{\bullet-}$)]: Bluish black powder: mp 203–206 °C (dec); IR (KBr) 3100–2700, 2184, 2162, 1659, 1609, 1571, 1504 cm^{-1}; UV (KBr) 1644, 850, 624, 368, 258 nm; Anal. Calcd for $(C_{11}H_9N_2)(C_{12}H_4N_4)(H_2O)_{0.25}$: C, 73.45; H, 3.56; N, 22.35%. Found: C, 73.45; H, 3.39; N,

22.09%.

7-Bromo-1,6-DAP·H$^+$–TCNQ$^{\bullet-}$ Salt [(6b·H$^+$)(TCNQ$^{\bullet-}$)]: Dark grayish green microcrystal: mp 232–235 °C (dec); IR (KBr) 3300–2800, 2178, 2155, 1651, 1603, 1579, 1499 cm^{-1}; UV (KBr) 1080(sh), 900, 784, 646, 360, 314, 264, 224 nm; Anal. Calcd for $(C_{11}H_8BrN_2)(C_{12}H_4N_4)$: C, 61.08; H, 2.67; N, 18.58%. Found: C, 60.97; H, 2.63; N, 18.33%.

7-Iodo-1,6-DAP·H$^+$–TCNQ$^{\bullet-}$ Salt [(6c·H$^+$)(TCNQ$^{\bullet-}$)]: Black powder: mp 206–207 °C (dec); IR (KBr) 3300–2800, 2182, 2174, 1645, 1598, 1577, 1504 cm^{-1}; UV (KBr) 1120(sh), 884, 666, 358, 215 nm; Anal. Calcd for $(C_{11}H_8IN_2)(C_{12}H_4N_4)(H_2O)_{0.25}$: C, 54.83; H, 2.50; N, 16.68%. Found: C, 54.66; H, 2.35; N, 16.61%.

7,9-Dichloro-2,5-dimethyl-1,6-DAP·H$^+$–TCNQ$^{\bullet-}$ Salt [(7a·H$^+$)(TCNQ$^{\bullet-}$)]: Dark purple powder: mp 223–228 °C (dec); IR (KBr) 3200–2700, 2181, 2158, 1617, 1577, 1507 cm^{-1}; UV (KBr) 1200(sh), 870, 766, 678, 376, 314, 268 nm; Anal. Calcd for $(C_{13}H_{11}Cl_2N_2)(C_{12}H_4N_4)$: C, 63.24; H, 3.29; N, 17.70%. Found: C, 63.41; H, 3.49; N, 17.47%.

7,9-Dichloro-2-methyl-5-phenyl-1,6-DAP·H$^+$–TCNQ$^{\bullet-}$ Salt [(7b·H$^+$)(TCNQ$^{\bullet-}$)]: Deep green powder: mp 182–185 °C (dec); IR (KBr) 3200–2500, 2186, 2157, 1639, 1610, 1577, 1505 cm^{-1}; UV (KBr) 1102, 870, 768, 632, 370, 314 nm; Anal. Calcd for $(C_{18}H_{13}Cl_2N_2)(C_{12}H_4N_4)(C_2H_6O)_{0.75}$: C, 66.73; H, 3.82; N, 14.82%. Found: C, 66.33; H, 3.41; N, 14.77%.

2:1 Salt of 7,9-Dichloro-2-methyl-5-phenyl-1,6-DAP·H$^+$–TCNQ$^{\bullet-}$ [(7b)(7b·H$^+$)(TCNQ$^{\bullet-}$)(H$_2$O)$_2$]. The solution of LiTCNQ (4.0 mg, 0.02 mmol) and the mixture of **7b** (3.2 mg, 0.01 mmol) and (**7b**·H$^+$)(Br$^-$) in MeOH (2 mL) were diffused at room temperature. Single crystals suitable for X-ray analysis were obtained as black needles. These crystals were obtained also by the aerial evaporation of a MeOH solution of (**7b**·H$^+$)(TCNQ$^{\bullet-}$): mp > 300 °C; IR (KBr) 3700–2500, 2189, 2161, 1637, 1606, 1577, 1543, 1507 cm^{-1}; UV (KBr) 1720(sh), 864, 762, 617, 370, 290 nm; Anal. Calcd for $(C_{18}H_{13}Cl_2N_2)(C_{18}H_{12}Cl_2N_2)(C_{12}H_4N_4)(H_2O)_2$: C, 64.37; H, 3.71; N, 12.51%. Found: C, 64.91; H, 3.74; N, 12.46%.

7,9-Dichloro-2-methyl-5-(2′-pyridyl)-1,6-DAP·H$^+$–TCNQ$^{\bullet-}$ Salt [(7c·H$^+$)(TCNQ$^{\bullet-}$)]: Dark green powder: mp 238–240 °C (dec); IR (KBr) 3200–2500, 2186, 2157, 1638, 1606, 1586, 1572, 1506 cm^{-1}; UV (KBr) 1100, 874, 768, 698, 526, 496, 386 nm; Anal. Calcd for $(C_{17}H_{12}Cl_2N_3)(C_{12}H_4N_4)(H_2O)_{0.25}$: C, 64.76; H, 3.09; N, 18.23%. Found: C, 64.88; H, 3.00; N, 18.03%.

1,6-DAP–TCNQ Complex [(6a)(TCNQ)]. Typical Procedure for the Preparation of TCNQ Complexes of DAPs. The 1,6-DAP (**6a**) (22.0 mg, 0.13 mmol) was placed in a 50-mL round-bottomed flask and dissolved with hot $CHCl_3$ (30 mL). TCNQ (25.3 mg, 0.12 mmol) in $CHCl_3$ (20 mL) was added to the mixture. After being stirred at the same temperature for 5 min, the mixture was gradually cooled down to room temperature and left standing for 12 h. The resulting powder was collected by filtration and washed with $CHCl_3$ (5 mL) to give the CT complex (33.8 mg) as a greenish black powder. mp > 300 °C; IR (KBr) 2197, 2168, 2120, 1657, 1599, 1540 cm^{-1}; UV (KBr) 864, 610, 356 nm; Anal. Calcd for $(C_{11}H_8N_2)(C_{12}H_4N_4)(H_2O)_{0.7}$: C, 71.75; H, 3.51; N, 21.83%. Found: C, 71.48; H, 3.15; N, 21.55%.

1,3-DAP–TCNQ Complex [(5a)$_3$(TCNQ)$_2$]: Olive black powder: mp > 300 °C; IR (KBr) 3700–2400, 2183, 2155, 1653, 1569, 1506 cm^{-1}; UV (KBr) 1150(sh), 864, 756, 622, 358, 232 nm; Anal. Calcd for $(C_{11}H_8N_2)_3(C_{12}H_4N_4)_2(H_2O)_{4.1}$: C, 69.38; H, 4.15; N, 19.87%. Found: C, 69.02; H, 3.42; N, 19.81%.

2-Phenyl-1,3-DAP–TCNQ Complex [(5b)$_3$(TCNQ)$_2$]: Deep yellowish green powder: mp > 300 °C; IR (KBr) 3700–2600, 2183, 2124, 1658, 1636, 1597, 1579, 1505 cm^{-1}; UV (KBr) 858, 762, 666, 352, 230 nm; Anal. Calcd for $(C_{17}H_{12}N_2)_3(C_{12}H_4N_4)_2(H_2O)_2$: C, 76.52; H, 4.11; N, 16.66%. Found: C, 76.53; H, 3.75; N, 16.86%.

2-*t*-Butyl-1,3-DAP–TCNQ Complex [(5c)(TCNQ)$_2$]: Grayish green powder: mp 188–193 °C (dec); IR (KBr) 2200, 2180, 2158, 1660, 1636, 1560, 1503 cm^{-1}; UV (KBr) 1000(sh), 856, 758, 632, 362, 216 nm; Anal. Calcd for $(C_{15}H_{16}N_2)(C_{12}H_4N_4)_2(H_2O)_{0.8}$: C, 72.39; H, 3.99; N, 21.65%. Found: C, 72.64; H, 3.82; N, 21.38%.

7-Bromo-1,6-DAP–TCNQ Complex [(6b)(TCNQ)]: Black powder: mp > 300 °C; IR (KBr) 2196, 2163, 1648, 1600, 1560 cm^{-1}; UV (KBr) 1010(sh), 866, 776, 606, 360, 266 nm; Anal. Calcd for $(C_{11}H_7BrN_2)(C_{12}H_4N_4)(H_2O)_{1.5}$: C, 57.76; H, 2.95; N, 17.57%. Found: C, 57.82; H, 2.65; N, 17.66%.

7-Methoxy-1,6-DAP–TCNQ Complex [(6d)(TCNQ)]: Black powder: mp > 300 °C; IR (KBr) 2199, 2180, 1661, 1586, 1504 cm^{-1}; UV (KBr) 870, 776, 664, 496, 368, 268 nm; Anal. Calcd for $(C_{12}H_{10}N_2O)(C_{12}H_4N_4)(H_2O)_{1.2}$: C, 67.98; H, 3.90; N, 19.82%. Found: C, 67.62; H, 3.39; N, 19.55%.

7,9-Dichloro-2,5-dimethyl-1,6-DAP–TCNQ Complex [(7a)$_3$(TCNQ)]: Dark yellow green powder: mp > 300 °C; IR (KBr) 2203, 2175, 1636, 1614, 1548, 1519 cm^{-1}; UV (KBr), 1000(sh), 868, 778, 368, 266 nm; Anal. Calcd for $(C_{13}H_{10}Cl_2N_2)_3(C_{12}H_4N_4)(H_2O)_{3.5}$: C, 57.64; H, 3.89; N, 13.18%. Found: C, 57.51; H, 3.79; N, 13.51%.

7,9-Dichloro-2-methyl-5-phenyl-1,6-DAP–TCNQ Complex [(7b)$_5$(TCNQ)$_6$]: Brownish black powder: mp > 300 °C; IR (KBr) 2003, 2184, 1692, 1615, 1551 cm^{-1}; UV (KBr) 956, 866, 772, 370, 298 nm; Anal. Calcd for $(C_{18}H_{12}Cl_2N_2)_5(C_{12}H_4N_4)_6(H_2O)_5$: C, 65.93; H, 3.21; N, 16.14%. Found: C, 66.12; H, 3.00; N, 16.03%.

7,9-Dichloro-2-methyl-5-(2′-pyridyl)-1,6-DAP–TCNQ Complex [(7c)$_2$(TCNQ)$_3$]: Black powder: mp > 300 °C; IR (KBr) 2200, 2106, 1636, 1615, 1558, 1520 cm^{-1}; UV (KBr) 1020(sh), 868, 780, 488, 370, 310 nm; Anal. Calcd for $(C_{17}H_{11}Cl_2N_3)_2(C_{12}H_4N_4)_3(H_2O)$: C, 65.33; H, 2.82; N, 19.59%. Found: C, 65.14; H, 3.03; N, 19.43%.

This work was partially supported by a Grant-in-Aid for Scientific Research (Nos. 14044059 and 16350074) from the Ministry of Education, Culture, Sports, Science and Technology, Japan, by PREST-JST and by the 21st Century COE program "Creation of Integrated EcoChemistry of Osaka University."

References

1 Preliminary accounts of a part of this work: a) K. Tamaki, Y. Morita, J. Toyoda, H. Yamochi, G. Saito, K. Nakasuji, *Tetrahedron Lett.* **1997**, *38*, 4583. b) Y. Morita, T. Murata, K. Tamaki, H. Yamochi, G. Saito, K. Nakasuji, *Synth. Met.* **2003**, *135–136*, 657.

2 a) D. H. Reid, *Chem. Ind.* **1956**, 1504. b) P. B. Sogo, M. Nakazaki, M. Calvin, *J. Chem. Phys.* **1957**, *26*, 1343.

3 For recent overview, see: a) *Molecular Magnetism*, ed. by K. Itoh, M. Kinoshita, Kodansha and Gordon and Breach Science Publishers, **2000**, pp. 1–347. b) *Magnetic Properties of Organic Materials*, ed. by P. M. Lahti, Marcel Dekker, New York, **1999**, pp. 1–728.

4 For recent overview, see: a) J. M. Williams, J. R. Ferraro,

R. J. Thorn, K. D. Carlson, U. Geiser, H. H. Wang, A. M. Kini, M.-H. Whangbo, *Organic Superconductors (Including Fullerenes)*, Prentice Hall, New Jersey, **1992**. b) T. Ishiguro, K. Yamaji, G. Saito, *Organic Superconductors*, 2nd ed., Springer-Verlag, Berlin, Heidelberg, **1998**. c) *TTF Chemistry: Fundamental and Applications of Tetrathiafulvalene*, ed. by J. Yamada, T. Sugimoto, Kodansha and Springer, Tokyo, **2004**.

5 a) R. C. Haddon, *Nature* **1975**, *256*, 394. b) R. C. Haddon, *Aust. J. Chem.* **1975**, *28*, 2343.

6 R. C. Haddon, F. Wudl, M. L. Kaplan, J. H. Marshall, R. E. Cais, F. B. Bramwell, *J. Am. Chem. Soc.* **1978**, *100*, 7629.

7 a) X. Chi, M. E. Itkis, B. O. Patrick, T. M. Barclay, R. W. Reed, R. T. Oakley, A. W. Cordes, R. C. Haddon, *J. Am. Chem. Soc.* **1999**, *121*, 10395. b) X. Chi, M. E. Itkis, K. Kirschbaum, A. A. Pinkerton, R. T. Oakley, A. W. Cordes, R. C. Haddon, *J. Am. Chem. Soc.* **2001**, *123*, 4041. c) M. E. Itkis, X. Chi, A. W. Cordes, R. C. Haddon, *Science* **2002**, *296*, 1443. d) S. K. Pal, M. E. Itkis, R. W. Reed, R. T. Oakley, A. W. Cordes, F. S. Tham, T. Siegrist, R. C. Haddon, *J. Am. Chem. Soc.* **2004**, *126*, 1478. e) S. K. Pal, M. E. Itkis, F. S. Tham, R. W. Reed, R. T. Oakley, R. C. Haddon, *Science* **2005**, *309*, 281.

8 a) T. Kubo, K. Yamamoto, K. Nakasuji, T. Takui, I. Murata, *Angew. Chem., Int. Ed. Engl.* **1996**, *35*, 439. b) T. Kubo, K. Yamamoto, K. Nakasuji, T. Takui, I. Murata, *Bull. Chem. Soc. Jpn.* **2001**, *74*, 1999. c) K. Nakasuji, T. Kubo, *Bull. Chem. Soc. Jpn.* **2004**, *77*, 1791. d) T. Kubo, M. Sakamoto, M. Akabane, Y. Fujiwara, K. Yamamoto, M. Akita, K. Inoue, T. Takui, K. Nakasuji, *Angew. Chem., Int. Ed.* **2004**, *43*, 6474. Highly conductive delocalized singlet biradical hydrocarbon based on the phenalenyl system, see: e) T. Kubo, A. Shimizu, M. Sakamoto, M. Uruichi, K. Yakushi, M. Nakano, D. Shiomi, K. Sato, T. Takui, Y. Morita, K. Nakasuji, *Angew. Chem., Int. Ed.* **2005**, *44*, 6564.

9 K. Nakasuji, M. Yamaguchi, I. Murata, K. Yamaguchi, T. Fueno, H. Ohya-Nishiguchi, T. Sugano, M. Kinoshita, *J. Am. Chem. Soc.* **1989**, *111*, 9265. We found that cationic salt (**4d**)-$(ClO_4^-)_{0.7}$, prepared as a paramagnetic stable salt, showed relatively high conductivity ($\approx 10^{-5}\,S\,cm^{-1}$).

10 a) K. Goto, T. Kubo, K. Yamamoto, K. Nakasuji, K. Sato, D. Shiomi, T. Takui, M. Kubota, T. Kobayashi, K. Yakushi, J. Ouyang, *J. Am. Chem. Soc.* **1999**, *121*, 1619. b) K. Fukui, K. Sato, D. Shiomi, T. Takui, K. Ito, K. Goto, T. Kubo, K. Yamamoto, K. Nakasuji, A. Naito, *Synth. Met.* **1999**, *103*, 2257. c) Y. Takano, T. Taniguchi, H. Isobe, T. Kubo, Y. Morita, K. Yamamoto, K. Nakasuji, T. Takui, K. Yamaguchi, *Chem. Phys. Lett.* **2002**, *358*, 17. d) Y. Takano, T. Taniguchi, H. Isobe, T. Kubo, Y. Morita, K. Yamamoto, K. Nakasuji, T. Takui, K. Yamaguchi, *J. Am. Chem. Soc.* **2002**, *124*, 11122. e) S. Suzuki, Y. Morita, K. Fukui, K. Sato, D. Shiomi, T. Takui, K. Nakasuji, *J. Am. Chem. Soc.* **2006**, *128*, 2530.

11 3-Oxophenalenoxyl: a) K. Hatanaka, Y. Morita, T. Ohba, K. Yamaguchi, T. Takui, M. Kinoshita, K. Nakasuji, *Tetrahedron Lett.* **1996**, *37*, 873. b) Y. Morita, S. Nishida, J. Kawai, K. Fukui, S. Nakazawa, K. Sato, D. Shiomi, T. Takui, K. Nakasuji, *Polyhedron* **2003**, *22*, 2209. Topological effect on spin distribution: c) Y. Morita, J. Kawai, K. Fukui, S. Nakazawa, K. Sato, D. Shiomi, T. Takui, K. Nakasuji, *Org. Lett.* **2003**, *5*, 3289. 6-Oxophenalenoxyl: d) K. Hatanaka, Y. Morita, T. Ohba, K. Yamaguchi, T. Takui, M. Kinoshita, K. Nakasuji, *Tetrahedron Lett.* **1996**, *37*, 877. e) Y. Morita, T. Ohba, N. Haneda, S. Maki, J. Kawai, K. Hatanaka, K. Sato, D. Shiomi, T. Takui, K. Nakasuji, *J. Am. Chem. Soc.* **2000**, *122*, 4825. f) Y. Morita, S. Maki, K. Fukui, T. Ohba, J. Kawai, K. Sato, D. Shiomi, T. Takui, K. Nakasuji, *Org. Lett.* **2001**, *3*, 3099. g) Y. Morita, J. Kawai, N. Haneda, S. Nishida, K. Fukui, S. Nakazawa, D. Shiomi, K. Sato, T. Takui, T. Kawakami, K. Yamaguchi, K. Nakasuji, *Tetrahedron Lett.* **2001**, *42*, 7991. h) S. Nishida, Y. Morita, K. Fukui, K. Sato, D. Shiomi, T. Takui, K. Nakasuji, *Angew. Chem., Int. Ed.* **2005**, *44*, 7277. Redox-based spin diversity: i) Y. Morita, S. Nishida, J. Kawai, K. Fukui, S. Nakazawa, K. Sato, D. Shiomi, T. Takui, K. Nakasuji, *Org. Lett.* **2002**, *4*, 1985. j) Y. Morita, S. Nishida, N. Oguchi, J. Kawai, K. Fukui, S. Nakazawa, K. Sato, D. Shiomi, T. Takui, K. Nakasuji, *Synth. Met.* **2003**, *137*, 1207. k) Y. Morita, J. Kawai, S. Nishida, N. Haneda, K. Fukui, K. Sato, D. Shiomi, T. Takui, K. Nakasuji, *Synth. Met.* **2003**, *137*, 1217.

12 J. Inoue, K. Fukui, T. Kubo, S. Nakazawa, K. Sato, D. Shiomi, Y. Morita, K. Yamamoto, T. Takui, K. Nakasuji, *J. Am. Chem. Soc.* **2001**, *123*, 12702.

13 a) K. Fukui, T. Aoki, Y. Morita, S. Nakazawa, K. Tamaki, K. Yamamoto, K. Sato, D. Shiomi, A. Naito, T. Takui, K. Nakasuji, *Synth. Met.* **2001**, *121*, 1770. b) Y. Morita, T. Aoki, K. Fukui, S. Nakazawa, K. Tamaki, S. Suzuki, A. Fuyuhiro, K. Yamamoto, K. Sato, D. Shiomi, A. Naito, T. Takui, K. Nakasuji, *Angew. Chem., Int. Ed.* **2002**, *41*, 1793. c) Y. Morita, S. Suzuki, J. Kawai, S. Nishida, K. Fukui, S. Nakazawa, K. Sato, D. Shiomi, T. Takui, K. Nakasuji, *Synth. Met.* **2003**, *137*, 1209. d) Y. Morita, S. Suzuki, K. Fukui, S. Nakazawa, K. Sato, D. Shiomi, T. Takui, K. Nakasuji, *Polyhedron* **2003**, *22*, 2215. e) Y. Morita, K. Fukui, S. Suzuki, T. Aoki, S. Nakazawa, K. Tamaki, A. Fuyuhiro, K. Yamamoto, K. Sato, D. Shiomi, A. Naito, T. Takui, K. Nakasuji, *Polyhedron* **2003**, *22*, 2199.

14 F. Sachs, *Liebigs Ann. Chem.* **1909**, *365*, 53.

15 A. F. Pozharskii, I. S. Kashparov, P. J. Holls, V. G. Zaletov, *Khim. Geterotsikl. Soedin.* **1971**, 543.

16 a) A. F. Pozharskii, V. V. Dal'nikovskaya, *Russ. Chem. Rev.* **1981**, *50*, 816, and the references cited there in. b) L. Nyulászi, T. Pasinszki, J. Réffy, T. Veszprémi, J. Fabian, W. Thiel, *Struct. Chem.* **1990**, *1*, 367.

17 a) M. I. El-Sheikh, J.-C. Chang, J. M. Cook, *Heterocycles* **1978**, *9*, 1561. b) J.-C. Chang, M. I. El-Sheikh, J. M. Cook, *Heterocycles* **1979**, *12*, 903. c) J. C. Chang, M. El-Sheikh, A. Harmon, K. Avasthi, J. M. Cook, *J. Org. Chem.* **1981**, *46*, 4188. d) S.-J. Lee, J. M. Cook, *Heterocycles* **1981**, *16*, 2125. e) R. W. Weber, S.-J. Lee, S. Milosevich, W. B. England, J. M. Cook, *Can. J. Chem.* **1982**, *60*, 3049. f) L. A. Ezhova, L. S. Éfros, É. R. Zakhs, *Khim. Geterotsikl. Soedin.* **1972**, 205. g) É. R. Zakhs, L. A. Ezhova, N. A. Kuznetsova, L. S. Éfros, *Khim. Geterotsikl. Soedin.* **1972**, 1391.

18 Crystal structures of nine kinds of 1,3-DAP derivatives with H-bonding interactions have been reported, see: a) R. M. Claramunt, J. Dotor, D. Sanz, C. Foces-Foces, A. L. Llamas-Saiz, J. Elguero, R. Flammang, J. P. Morizur, E. Chapon, J. Tortajada, *Helv. Chim. Acta* **1994**, *77*, 121. b) C. Foces-Foces, A. L. Llamas-Saiz, R. M. Claramunt, D. Sanz, J. Dotor, J. Elguero, *J. Crystallogr. Spectrosc. Res.* **1993**, *23*, 305. c) A. L. Llamas-Saiz, C. Foces-Foces, D. Sanz, R. M. Claramunt, J. Dotor, J. Elguero, J. Catalan, J. C. del Valle, *J. Chem. Soc., Perkin Trans. 2* **1995**, 1389. d) T. Yokoyama, T. Masuo, H. Akashi, M. Zenki, *Bull. Chem. Soc. Jpn.* **1995**, *68*, 1331. e) S. M. Baker, R. G. Baughman, C. E. Meloan, P. Mumba, *Acta Crystallogr., Sect. C* **1996**, *52*, 998. f) S. Patnaik, K. Vishnumurthy, M. Sridhar, S. Chandrasekhar, K. Usha, T. N. G. Row, *Acta Crystallogr., Sect. C* **1997**, *53*, 130.

19 a) Only one example of crystal structure analysis for 1,6-DAP derivative has been performed, but its H-bonding nature was not discussed, see: Q. Ding, J. W. Lown, *Heterocycl. Com-*

mun. **1998**, *4*, 125. b) Crystal structures of 1,3,4,6,7,9-hexaazaphenalenyl system are also recently investigated, see: S. Suzuki, Y. Morita, K. Fukui, K. Sato, D. Shiomi, T. Takui, K. Nakasuji, *Inorg. Chem.* **2005**, *44*, 8197.

20 K. Nakasuji, K. Sugiura, T. Kitagawa, J. Toyoda, H. Okamoto, K. Okaniwa, T. Mitani, H. Yamamoto, I. Murata, A. Kawamoto, J. Tanaka, *J. Am. Chem. Soc.* **1991**, *113*, 1862.

21 Organic conductors with H-bonds, see: a) M. R. Bryce, *Chem. Soc. Rev.* **1991**, *20*, 355. b) M. R. Bryce, *J. Mater. Chem.* **1995**, *5*, 1481. c) P. Batail, K. Boubekeur, M. Fourmigué, J.-C. P. Gabriel, *Chem. Mater.* **1998**, *10*, 3005. d) M. Fourmigué, P. Batail, *Chem. Rev.* **2004**, *104*, 5379.

22 a) Y. Morita, T. Murata, H. Yamochi, G. Saito, K. Nakasuji, *Synth. Met.* **2003**, *135–136*, 579. b) T. Murata, Y. Morita, K. Fukui, K. Sato, D. Shiomi, T. Takui, M. Maesato, H. Yamochi, G. Saito, K. Nakasuji, *Angew. Chem., Int. Ed.* **2004**, *43*, 6343.

23 Y. Morita, E. Miyazaki, K. Fukui, S. Maki, K. Nakasuji, *Bull. Chem. Soc. Jpn.* **2005**, *78*, 2014.

24 a) Y. Morita, S. Maki, M. Ohmoto, H. Kitagawa, T. Okubo, T. Mitani, K. Nakasuji, *Org. Lett.* **2002**, *4*, 2185. b) M. Ohmoto, S. Maki, Y. Morita, H. Kitagawa, T. Okubo, T. Mitani, K. Nakasuji, *Synth. Met.* **2003**, *133–134*, 337. c) Y. Morita, S. Maki, M. Ohmoto, H. Kitagawa, T. Okubo, T. Mitani, K. Nakasuji, *Synth. Met.* **2003**, *135–136*, 541. d) E. Miyazaki, Y. Morita, Y. Umemoto, S. Maki, K. Nakasuji, *Chem. Lett.* **2005**, *34*, 1326.

25 Y. Morita, S. Maki, M. Hori, M. Ohmoto, E. Mochizuki, Y. Kai, H. Kitagawa, T. Mitani, K. Nakasuji, *Synth. Met.* **2003**, *135–136*, 537.

26 Y. Morita, E. Miyazaki, T. Yokoyama, T. Kubo, E. Mochizuki, Y. Kai, K. Nakasuji, *Synth. Met.* **2003**, *135–136*, 617.

27 a) Y. Morita, T. Murata, S. Yamada, M. Tadokoro, A. Ichimura, K. Nakasuji, *J. Chem. Soc., Perkin Trans. 1* **2002**, 2598. b) Y. Morita, T. Murata, K. Fukui, M. Tadokoro, K. Sato, D. Shiomi, T. Takui, K. Nakasuji, *Chem. Lett.* **2004**, *33*, 188. c) T. Murata, Y. Morita, Y. Nishimura, K. Nakasuji, *Polyhedron* **2005**, *24*, 2625. d) T. Murata, Y. Morita, K. Nakasuji, *Tetrahedron* **2005**, *61*, 6056. e) Y. Morita, T. Murata, K. Fukui, S. Yamada, K. Sato, D. Shiomi, T. Takui, H. Kitagawa, H. Yamochi, G. Saito, K. Nakasuji, *J. Org. Chem.* **2005**, *70*, 2739.

28 V. Paragamian, M. B. Baker, B. M. Puma, J. Reale, Jr., *J. Heterocycl. Chem.* **1968**, *5*, 591.

29 W. A. Mosher, T. E. Banks, *J. Org. Chem.* **1971**, *36*, 1477.

30 E. Roberts, E. E. Turner, *J. Chem. Soc.* **1927**, 1832.

31 C. P. Brock, J. D. Dunitz, *Acta Crystallogr., Sect. B* **1982**, *38*, 2218.

32 A. Bondi, *J. Phys. Chem.* **1964**, *68*, 441.

33 a) J. B. Torrance, B. A. Scott, B. Welber, F. B. Kaufman, P. E. Seiden, *Phys. Rev. B* **1979**, *19*, 730. b) E. M. Conwell, I. A. Howard, J. P. Pouget, C. S. Jacobsen, J. C. Scott, L. Zuppiroli, *Semiconductors and Semimetals*, ed. by E. M. Conwell, Academic Press, Inc., New York, **1988**, Vol. 27. c) J. Tanaka, M. Tanaka, T. Kawai, T. Takabe, O. Maki, *Bull. Chem. Soc. Jpn.* **1976**, *49*, 2358. d) J. B. Torrance, B. A. Scott, F. B. Kaufman, *Solid State Commun.* **1975**, *17*, 1369.

34 J. S. Chappell, A. N. Bloch, W. A. Bryden, M. Maxfield, T. O. Poehler, D. O. Cowan, *J. Am. Chem. Soc.* **1981**, *103*, 2442.

35 a) C. J. Fritchie, P. Arthur, *Acta Crystallogr.* **1966**, *21*, 139. b) K. D. Cummings, D. B. Tanner, J. S. Miller, *Phys. Rev. B* **1981**, *24*, 4142.

36 a) P. S. Flandrois, D. Chasseau, *Acta Crystallogr., Sect. B* **1977**, *33*, 2744. b) T. J. Kistenmacher, T. J. Emge, A. N. Bloch, D. O. Cowan, *Acta Crystallogr., Sect. B* **1982**, *38*, 1193.

37 a) G. Saito, S. Hirate, K. Nishimura, H. Yamochi, *J. Mater. Chem.* **2001**, *11*, 723. b) S.-S. Pac, G. Saito, *J. Solid State Chem.* **2002**, *168*, 486.

38 G. M. Sheldrick, *Crystallographic Computing 3*, ed. by G. M. Sheldrick, C. Kruger, R. Goddard, Oxford University Press, **1985**, pp. 175–189.

39 G. M. Sheldrick, *Program for the Solution of Crystal Structuers*, University of Göettingen, Germany, **1997**.

40 P. T. Beurskens, G. Admiraal, G. Beurskens, W. P. Bosman, R. de Gelder, R. Israel, J. M. M. Smits, *The DIRDIF-94 Program System: Technical Report of the Crystallography Laboratory*, University of Nijmegen, The Netherlands, **1994**.

41 G. M. Sheldrick, *Program for the Refinement of Crystal Structures*, University of Göettingen, Germany, **1997**.

42 *teXsan: Crystal Structure Analysis Package*, Molecular Structure Corporation, **1985** and **1999**.